Induction of the ALT pathway requires loss of ATRX-DAXX in concert with genotoxic lesions at telomeres

David Clynes (david.clynes@oncology.ox.ac.uk)
University of Oxford
Tomas Goncalves
University of Oxford https://orcid.org/0000-0002-3342-0461
Thomas Kent
University of Oxford
Sam Shepherd
University of Oxford
Siobhan Cunniffe
University of Oxford
Sangwoo Kim
University of Oxford https://orcid.org/0000-0002-2951-3331
Tim Humphrey
University of Oxford
Richard Gibbons
University of Oxford

Article

Keywords: ATRX, Glioma, Alternative lengthening of telomeres, Cancer, SETD2, DAXX, R-loops, Break Induced Replication

Posted Date: April 28th, 2021

DOI: https://doi.org/10.21203/rs.3.rs-362334/v1

Induction of the ALT pathway requires loss of ATRX-DAXX in concert with genotoxic lesions at telomeres

Tomas Goncalves[1,3#], Thomas Kent[1,3#], Sam Shepherd[1,2], Siobhan Cunniffe[1,2], Sangwoo Kim[1,2], Timothy C. Humphrey[2], Richard J. Gibbons[3], David Clynes[1,2*]

[1] MRC Weatherall Institute of Molecular Medicine, University of Oxford, John Radcliffe Hospital, Oxford OX3 9DS, UK.

[2] MRC Oxford Institute for Radiation Oncology, Department of Oncology, University of Oxford, Oxford OX3 7DQ, UK

[3] MRC Molecular Haematology Unit, MRC Weatherall Institute of Molecular Medicine, University of Oxford, John Radcliffe Hospital, Oxford OX3 9DS, UK

#These authors contributed equally to this work

*Correspondence: david.clynes@oncology.ox.ac.uk Tel: 0044 1865 222440

ABSTRACT

A key requisite for indefinite growth of cancer cells is the ability to continuously elongate telomeres to circumvent the onset of senescence or apoptosis. In approximately 10 – 15% of cancers this is achieved through the Alternative Lengthening of Telomeres (ALT) pathway, a Break Induced Replication (BIR) mediated mechanism of telomere copying. ATRX has emerged as the key tumour suppressor in ALT cancers but its loss is insufficient to drive induction of the pathway. Here, we report that depletion of ATRX and/or DAXX in the presence of various genotoxic agents is sufficient to induce ALT. Moreover, co-deletion of ATRX and SETD2, commonly mutated in high grade gliomas (HGGs), elicits induction of ALT. Mechanistically, SETD2 restricts the accumulation of telomeric R-loops, which, in the absence of ATRX, leads to fork collapse and the loss of telomere sister chromatid cohesion. Cumulatively this provides a substrate for out of register BIR and telomere lengthening.

KEYWORDS

ATRX, Glioma, Alternative lengthening of telomeres, Cancer, SETD2, DAXX, R-loops, Break Induced Replication

Due to the inherent inability of DNA polymerases to fully replicate the distal ends of linear chromosomes, chromosomal DNA is progressively shortened with each round of cell division. To circumvent potentially detrimental effects to genome stability and loss of genetic information, humans, like many other species, have developed specialised nucleoprotein structures, called telomeres, that are comprised of many kilobases (kb) of a tandem repeat sequence, TTAGGG, culminating in a 3' protrusion of single stranded G-rich DNA of 50 – 400 nucleotides. Telomeric sequence is bound by a specialised protein complex, denoted Shelterin, which comprises the proteins TRF1, TRF2, POT1, TIN1, TPP1 and RAP1 [1]. Telomeres range from 3 to 12 kb in humans and progressively shorten by about 200 base pairs per cell division due to the end-replication problem. Once telomeres reach a critical length, termed the 'Hayflick limit', they elicit DNA damage checkpoint activation, leading to cellular senescence or telomere-induced apoptosis. A key hallmark of cancer cells is their ability to circumvent telomere shortening via a telomere length maintenance mechanism (TMM). In the majority of cancers, this is achieved through the upregulation of telomerase, a specialised ribonucleoprotein that acts to progressively add telomeric repeats to the end of chromosomes. More recently it has emerged that approximately 15% of cancers maintain telomere length through a telomerase independent TMM, known as the Alternative Lengthening of Telomeres (ALT) pathway. The ALT pathway is particularly prevalent in cancers of mesenchymal origin, including several cancers of the central nervous system (CNS), with rates as high as 63% [2]. ALT in human cancer cells is generally considered to be a form of aberrant telomere recombination and conservative DNA synthesis known as Break Induced Replication (BIR), occurring during both the G2 and Mitosis phases of the cell cycle. A three-protein axis has been implicated in facilitating ALT-mediated telomere synthesis; POLD3, PCNA and RAD52 [3–5]. A second Rad52 independent pathway has also recently been reported,

61 suggesting that ALT is in fact a bifurcated pathway, with similarities to telomerase
62 independent telomere maintenance pathways originally described in budding yeast [6,7].
63
64 Further work in human cells has suggested that replication stress arising at telomeres can
65 potentiate the ALT pathway [4]. Indeed, owing to their repetitive nature, telomeres are thought
66 to be inherently difficult sequences to replicate and telomeres have been shown to
67 phenotypically resemble common fragile sites due to the overt fragility they exhibit under
68 conditions of replication stress [8]. This is likely in large part due to the propensity of the G-rich
69 repetitive telomeric sequence to adopt non-canonical DNA secondary structures, including
70 the G-quadruplex (G4) conformation and R-loops; three-stranded nucleic acid structures
71 consisting of an RNA:DNA hybrid and a displaced piece of single stranded DNA [9]. In line with
72 this notion, abrogation of FANCM activity, which has known roles in R-loop resolution and
73 fork stabilisation [10–12], or depletion of RNase H, which can degrade DNA:RNA hybrids, have
74 both recently been shown to potentiate markers of the ALT pathway [10,13,14]
75
76 A near unifying feature of ALT positive cancer cells is loss of the alpha thalassemia/mental
77 retardation syndrome X-linked chromatin remodeller (ATRX) and/or its interaction partner
78 DAXX (death domain-associated protein) [2,15,16]. Indeed, previous work by our lab and others
79 has demonstrated that ectopic expression of ATRX leads to a DAXX-dependent suppression
80 of the ALT pathway [17,18]. Of note, depletion or knockout (KO) of ATRX in telomerase positive
81 or primary cell lines is generally insufficient to induce markers of the ALT pathway [15,17,19,20],
82 with the notable exception of a minority of glioma cell lines [21]. A likely explanation for these
83 observations is that other genetic or epigenetic events are required for the induction of ALT

84 in human cancer in concert with ATRX loss. To date, what these events are remains
85 contentious.
86
87 ATRX is a chromatin remodelling factor of the Snf2 family (reviewed in [22] which, together with
88 the histone chaperone DAXX, facilitates the incorporation of the histone variant H3.3 into
89 defined genomic sites, including telomeric chromatin, in a replication independent chromatin
90 assembly pathway [23–25]. In the last decade, a number of studies have implicated ATRX in a
91 plethora of roles related to the maintenance of genome stability. One major role of ATRX
92 appears to be the regulation of non-canonical DNA secondary structures, with ATRX null cells
93 displaying increases in both G4 and R-loop structures [26,27]. ATRX also has multiple reported
94 roles in DNA replication; including the prevention of replication fork stalling, potentiation of
95 fork restart and the prevention of excessive nucleolytic degradation of stalled forks [20,28–30].
96 Additionally, evidence exists for a role of ATRX in facilitating DNA double strand break (DSB)
97 repair, with roles reported in both the major DSB repair pathways, homologous
98 recombination (HR) [31,32] and non-homologous end joining (NHEJ) [33]. Which of these role(s)
99 are required for ATRX to prevent either the induction or maintenance of the ALT pathway is
100 to date unclear.
101
102 Here, we report on an overarching role for ATRX in the suppression of the ALT pathway.
103 Firstly, we demonstrate that ATRX/DAXX is required to prevent ALT in the presence of a
104 variety of genotoxic agents that are known to result in replication fork stalling and reversal.
105 Induction of the ALT phenotype is associated with increases in telomeric DNA damage and
106 single stranded DNA, in addition to a loss of sister chromatid telomere cohesion. Based on
107 this we propose that the induction of ALT in cancer cells requires two independent events;

one involving a mutation (or mutations) in a factor (or factors) that leads to the generation of replicative stress at telomeres, which, if in concert with ATRX loss, leads to both fork collapse and the loss of telomere sister chromatid cohesion. This cumulatively results in out of register BIR and telomere lengthening. We demonstrate one such factor to be the histone methyltransferase SETD2, which is frequently mutated concomitantly with ATRX in high grade gliomas (HGGs), by showing that loss of SETD2 elicits induction of the ALT pathway, specifically in the absence of ATRX, via the generation of telomeric R-loops.

RESULTS

Loss of ATRX does not confer activation of the ALT pathway in telomerase positive cell lines

Previous work has reported that depletion or KO of ATRX in telomerase positive or primary cell lines is insufficient to induce markers of the ALT pathway [15,17,19,20], with the notable exception of a minority of glioma cell lines [21]. One implication of these findings is that the loss of ATRX, while generally a requisite for ALT pathway induction and/or maintenance, must occur in concert with other genomic events within cancer cells that cumulatively lead to telomere lengthening via ALT. We therefore sought to explore this possibility further.

The HeLa long telomere cell line (henceforth referred to as HeLa LT) is a subclone of HeLa with long telomeres (~20 kb) which has previously shown to be amenable to ALT induction through depletion of ASF1 [34]. Consistent with previous reports, two independent ATRX CRISPR-Cas9 KO HeLa LT clones (Figure 1A) conferred sensitivity to a variety of genotoxic agents known to induce replicative stress, including the G4 stabilising ligand pyridostatin (PDS), aphidicolin (APH) and hydroxyurea (HU) (Figures S1A-C). Despite these conferred synthetic lethal interactions, neither of the KO clones elicited an increase in cardinal ALT markers, including C-circles (Figures 1B and 1C), ALT-associated PML nuclear bodies (APBs) (Figures 1D and 1E) or telomere length heterogeneity (Figure 1F).

Treatment with the G-quadruplex stabilising ligand PDS confers activation of the ALT pathway in the absence of ATRX

A key feature of telomeres is their propensity to adopt non-canonical DNA secondary structures, including the G4 conformation, which has been implicated in both transcriptional dysregulation and DNA damage [35]. ATRX binds widely at sites in the genome predicted to form G4 structures, including telomeres [25,36] and ATRX loss confers sensitivity to various G4 stabilising ligands, including PDS (Figure S1A), suggesting that ATRX protects G4 sites from genome instability [26,30]. In accordance with this, we observe that the addition of PDS led to an increase in ATRX recruitment to telomeres (Figures S2A and S2B), suggestive of a putative role for ATRX in protecting telomeric DNA upon the stabilisation of G4s. To explore this possibility further, we treated our two HeLa LT KO clones with PDS and assessed for markers of activation of the ALT pathway. Strikingly, treatment with PDS elicited an increase in many of these cardinal markers, including C-circles (Figures 2A and 2B) and the formation of APBs (Figures 2C and 2D) to levels comparable to the archetypical ALT cell line U-2 OS, whereas no notable increase was observed in the ATRX wildtype cells. Addition of PDS also elicited a decrease in total telomere number and an increase in telomere intensity, consistent with increased telomere clustering and telomere synthesis (Figures S3A and S3B).

ALT has been suggested to be coincident with telomeric replicative stress, with an accumulation of RPA2 at telomeres upon ALT induction [34] and an increase in single stranded telomeric DNA (ssTel), as detected by non-denaturing telomeric FISH [37]. Consistent with these findings, an ALT specific co-localisation between RPA and ssTel is clearly detectable across a panel of cell lines (Figures S4A and S4B). This signal was refractory to RNase A and RNase H

164 treatment, confirming that the ssTel signal was detecting telomeric DNA and not TERRA RNA
165 (Figure S4C). Inducible expression of ATRX in ALT positive U-2 OS cells, using our previously
166 characterised U-2 OS^{ATRX} cell line [18] led to a complete abrogation of RPA ssTel foci, once again
167 confirming RPA/ssTel as a bona-fide ALT marker and suggesting that the signal is a
168 consequence of ATRX loss in ALT cancer cells (Figure S4B). We next asked whether treatment
169 of our Hela LT ATRX KO clones with PDS also induced formation of this novel ALT marker. As
170 expected, addition of PDS significantly increased detectable RPA ssTel foci in both
171 independent ATRX KO clones, with no detectable increase in wildtype ATRX HeLa LT cells
172 (Figures 2E and 2F). ALT positive cell lines characteristically exhibit long and heterogeneous
173 telomere lengths [38]. Consistent with a bona fide induction of the ALT pathway, treatment with
174 PDS led to a characteristic lengthening and spread of telomere lengths in the ATRX KO clones
175 but not in the ATRX wildtype cells (Figure 2G). We also used monochrome multiplex qPCR
176 (mm-qPCR) analysis to show that the T/S ratio – the telomere repeat number normalised to
177 the single copy gene *HBB* (encoding beta-globin) – significantly increased after PDS treatment
178 in both ATRX KO clones but not in the wildtype cells (Figure S5A), again highly suggestive of a
179 bona fide induction of the ALT pathway and associated telomere synthesis in these cells.
180
181 *Induction of ALT in the absence of ATRX upon PDS treatment is dependent on the Mus81*
182 *endonuclease*
183
184 It has been hypothesised that ALT emanates from the formation of a DSB within the telomere
185 sequence, likely attributable to the stalling, reversal, and subsequent collapse of replication
186 forks. Consistent with an induction of an ALT like process and fork collapse events, loss of
187 ATRX was associated with a significant increase in telomere-associated ATM,

188 autophosphorylated at serine 1981 (pATM S1981), a marker of ATM activation at DNA DSBs
189 [39] (Figures 3A and 3B). The cleavage of stalled forks to generate a DSB is dependent on the
190 activity of the structure-selective endonuclease MUS81-EME2 [40] and, in agreement with a
191 central role for replication fork collapse in the initiation of ALT, MUS81 activity is a requisite
192 for telomere maintenance in ALT cells [40,41]. We next sought to explore whether the
193 destabilisation and collapse of replication forks was a feature of ALT induction upon the
194 addition of PDS to our ATRX KO cells. Consistent with this requirement, knockdown of Mus81
195 completely abrogated the increase in C-circles observed in the ATRX KO cells upon PDS
196 treatment (Figures 3C and 3D). Likewise, the depletion of Mus81 was also associated with an
197 attenuation of RPA ssTel foci in the ATRX KO cells (Figures 3E and 3F). Taken together, we
198 conclude that the generation of ALT upon ATRX loss and PDS treatment is likely attributable
199 to an increased destabilisation and Mus81-dependent processing of replication forks in the
200 absence of ATRX, which in turn generates the DSB substrate for subsequent BIR-mediated
201 lengthening of telomeres.
202
203 *Genotoxic agents that cause replicative stress induce markers of ALT in ATRX deficient cells*
204
205 Recent work has shown that replication fork uncoupling and reversal is a global response to
206 a plethora of genotoxic agents that can cause adducts or lesions on DNA [42]. Given the reported
207 roles for ATRX in promoting replication fork processivity and stability [20,28,29], we considered
208 the possibility that the addition of a panel of genotoxic agents at sublethal doses, which on
209 their own are reported to induce fork remodelling but not collapse, could also specifically
210 elicit ALT in the absence of ATRX. Perturbations in fork processivity and reversal have been
211 extensively reported as a frequent event upon addition of the Topoisomerase I inhibitor

camptothecin (CPT) [43]. In agreement with the conjecture that ATRX is required to protect telomeres under conditions of replicative stress, addition of a low dose of CPT induced the formation of C-circles to levels almost equivalent to those found in the ALT positive U-2 OS cell line (Figure 4 A). Likewise, addition of CPT led to an increase in APBs (Figures 4B and 4C) and RPA ssTel foci (Figures 4D and 4E) as well as a significant increase in telomere length heterogeneity (Figure S5B), specifically in the ATRX KO clones, consistent with a bona fide induction of the ALT pathway. Interfacial inhibition of Topoisomerase II, through addition of etoposide (ETO), elicited a similar response, with preferential increases in C-circles (Figure 4A), APBs (Figures 4B and 4C) and RPA ssTel foci (Figures 4D and 4E) in ATRX deficient cells, albeit to a slightly lesser extent than that observed with CPT. Treatment with low doses of the DNA polymerase inhibitor APH, which has previously been shown to generate replicative stress at common fragile sites [8], elicited only a minimal increase C-circles which failed to reach significance (Figure 4A) and no detectable increase in APBs (Figures 4B and 4C) in the ATRX null cells, but surprisingly did lead to a notable increase in RPA ssTel foci (Figures 4D and 4E). Taken together, this data suggests that it is the formation of a lesion or structure on telomeric DNA, and not replication stress *per se*, that facilitates induction of the ALT pathway in the absence of ATRX.

To assess whether induction of ALT was specific to the HeLa LT cell line upon loss of ATRX, we sought to deplete ATRX via shRNA in a non-LT HeLa cell line with standard length telomeres (HeLa ST) (Figure S6A). Consistent with our previous observations in the HeLa LT cell line, addition of camptothecin (CPT), specifically in ATRX depleted cells, led to a robust augmentation of C-circles (Figures S6B and S6C), albeit to a lesser extent than that observed in the HeLa LT ATRX KO clones. Likewise, we found that addition of PDS led to induction of

another of the ALT hallmarks, the RPA ssTel foci, again only in the ATRX depleted cells (Figures S6D and S6E). Taken together, we conclude that the observed induction of ALT is not specific to the HeLa LT cell line, however, the presence of long telomeres does appear to exacerbate the response.

ATRX and DAXX function epistatically in the suppression of ALT

A minority of ALT cancers are characterised by a loss of the histone chaperone protein DAXX which, together with ATRX, forms a complex that can facilitate incorporation of the histone variant H3.3 into ribosomal [44], pericentromeric [23] and telomeric [24,25] chromatin. We have previously reported that the suppression of the ALT pathway through ectopic expression of ATRX is lost upon depletion of DAXX [18], suggesting that ATRX and DAXX likely work in concert in the suppression of ALT. To further explore the relationship between ATRX and DAXX in the suppression of the ALT pathway, CRISPR-Cas9 mediated DAXX KO clones in the HeLa LT cell line, both in the context of WT ATRX and ATRX KO, were generated (Figure 5A). Consistent with the notion that ATRX/DAXX function as a complex in the suppression of the ALT pathway, the loss of DAXX facilitated the accumulation of C-circles (Figures 5B and 5C), RPA ssTel foci (Figures 5D and 5E) and APBs (Figures 5F and 5G) upon treatment with both PDS and CPT. Importantly, the co-depletion of both ATRX and DAXX failed to confer any cumulative increase in these cardinal ALT markers (Figures 5B-G), strongly suggesting that both ATRX and DAXX are functioning within the same pathway in the suppression of telomeric replicative stress and the ALT pathway.

SETD2 loss in combination with ATRX loss triggers markers of the ALT pathway

Data presented here suggests that the induction of ALT in cancer cells in fact requires two independent events, involving mutations or factors that generate a telomeric structure or lesion, which, if in concert with ATRX loss, leads to fork collapse. This thereby provides the substrate and means for BIR and subsequent telomere lengthening.

Recurrent mutations in genes that disrupt the post-translational modification of histone H3 at H3 K36, including mutations in H3.3 G34R/V or the histone methyl transferase SETD2, are also frequently found in paediatric HGGs and are highly co-incident with mutations in ATRX [45]. Of note, mutations in SETD2 have recently been linked to the generation of replicative stress [46]. To explore the possibility that loss of ATRX, in the context of SETD2 loss, is sufficient to drive the ALT pathway, we generated SETD2 KO clones both in the context of wildtype ATRX and ATRX loss. Loss of SETD2 activity in the resulting clones was confirmed by a global loss of histone H3 K36me3 (Figure 6A). Loss of SETD2 alone was insufficient to elicit markers of ALT, however strikingly, the combination of both ATRX and SETD2 loss induced an accumulation of C-circles (Figures 6B and 6C), APBs (Figure 6D) and RPA ssTel foci (Figure 6E) akin to those observed in U-2 OS cells. The loss of SETD2 was associated with increases in DNA damage markers, including pATM, which were further exacerbated upon the combined KO of both SETD2 and ATRX (Figure 6F). Strikingly, this accumulation of C-circles was dramatically reduced upon treatment with the transcription inhibitor triptolide in a dose dependent manner (Figures 6G and S7A). We noted that treatment with triptolide elicited a minor effect on cell cycle distribution, with a slight increase in the percentage of cells in G1, however, in contrast to the dose dependency observed with the loss of C-circles, treatment with all 3

doses of triptolide elicited an identical change to the cell cycle distribution (Figures S7B-F). Taken together, it is therefore unlikely that the reduction in C-circles is an indirect consequence of changes to the cell cycle. Given this dependence on transcription and previous findings that the ALT pathway is potentiated through the formation of telomeric R-loops [10,12,13,47], we asked whether the depletion of SETD2 was associated with an increase in telomeric R-loops. Strikingly, immunoprecipitation using an antibody specific to RNA-DNA hybrids (S9.6) showed a marked accumulation of telomeric R-loops upon loss of SETD2 (Figure 6H). When cells were pre-treated with RNase H prior to immunoprecipitation, the signal was decreased, suggesting that the signal was indeed specific to the DNA-RNA hybrids (Figure 6H). We next sought to determine whether the accumulation of telomeric R-loops observed upon SETD2 loss was responsible for facilitating the accumulation of ALT markers in the combined ATRX SETD2 KO cells. To this end, we overexpressed the RNA-DNA endonuclease RNase H1 in HeLa LT SETD2 KO cells (Figure 6I) which led to a marked decrease in telomeric R-loops (Figure 6J). Moreover, overexpression of RNase H1 in the ATRX SETD2 KO cells resulted in a reduction of C-circles that was not observed upon overexpression of a catalytically dead mutant of RNase H1 (D210N) (Figure 6K). Taken together, this data supports a model whereby loss of SETD2 leads to the accumulation of telomeric R-loops which triggers the ALT pathway, specifically in the absence of ATRX.

ATRX is required for telomere sister chromatid cohesion

The repair of telomeric DNA DSBs by BIR is not exclusive to cancer cells dependent on the ALT pathway [3,48] and the use of a sister telomere as an in-register template will not result in a net elongation of telomeres. Prior reports have suggested that loss of ATRX leads to a diminution

of telomere cohesion [19,49], suggesting that ATRX may have an additional major role in the suppression of the ALT pathway, by ensuring the correct register of telomeric BIR. To this end, we sought to determine whether loss of ATRX in the HeLa LT cell line elicited a loss of telomeric cohesion using a FISH probe specific to the subtelomeric q arm of chromosome 13 (and an internal control probe mapping to 13q14). A loss of telomere cohesion was then scored in interphase cells as the appearance of a doublet as opposed to a single focus, with doublets indicative of a separation of sister telomeres. Strikingly, loss of ATRX resulted in a significant increase in the proportion of doublets, consistent with a premature loss of telomere sister chromatid cohesion in the absence of ATRX (Figures 7A and 7B). No significant changes were observed when using a FISH probe targeting an internal region of chromosome 13, suggesting that defective sister chromatid cohesion in the absence of ATRX was confined to telomeres (Figures 7A and 7B).

DISCUSSION

Loss of ATRX or its functional interaction partner DAXX are hallmarks of the vast majority of ALT cancer cells but, despite ectopic expression of ATRX being sufficient to suppress the pathway in ALT cells [17,18], the loss of ATRX is generally insufficient to induce markers of the ALT pathway [15,17,19,20]. Of note, recent work has shown that CRISPR-Cas9 mediated depletion of ATRX induces canonical markers of ALT in two specific glioma cell lines (U-251 and UW479) and a prostate cancer cell line (LAPC-4) [21,50]. Given that this induction was specific to these cell lines, it is likely that additional genetic or epigenetic events occur alongside ATRX loss to facilitate induction of ALT in human cancer. Consistent with this prediction, we report here that the loss of ATRX in HeLa cells failed to induce the canonical markers of ALT. It has been

suggested that the presence of telomeric replicative stress drives the ALT pathway, with the stalling and collapse of replication forks at telomeres leading to the generation of a one ended DSB which is subsequently repaired by BIR in G2 or mitosis (MiDAS) [4,7]. Loss of ATRX has previously been linked to the generation of replicative stress [20,28–30,51], however, given that loss of ATRX is generally insufficient to induce ALT, we reasoned that the parallel induction of telomeric replicative stress, which would normally be tolerated through the activity of ATRX/DAXX, could trigger the ALT pathway only when in concert with ATRX loss. In concordance with this notion, we show here that the treatment of ATRX deplete cells with genotoxic agents known to induce structures/lesions on DNA triggers multiple canonical markers of an active ALT pathway, specifically in the absence of ATRX and/or DAXX. Genotoxic agents that were found to induce ALT included the G4 stabilising ligand PDS, and the topoisomerase inhibitors ETO and CPT, both of which are frequently used in cancer therapy. Treatment with relatively mild doses of these drugs has been linked to fork slowing and reversal in the absence of chromosomal breakage [42], implying that under these conditions fork collapse is facilitated only upon ATRX and/or DAXX loss. In line with this, telomeric S1981 phosphorylated ATM was dramatically enriched at telomeres upon PDS treatment in ATRX null cells and the generation of ALT markers was dependent on the MUS81 endonuclease, suggesting that forks are cleaved and collapsed in the absence of ATRX upon PDS treatment. Importantly, we report that low dose APH treatment did not elicit the same response, implying that it is not replicative stress *per se* that elicits ALT in the absence of ATRX and/or DAXX, but more likely the presence of a 'lesion' or 'secondary structure' on telomeric DNA. Indeed, G4 structures have been proposed to form a barrier to the replisome, although in the case of telomeres the G4 structure would form on the lagging strand, which presumably constitutes less of a hindrance to the fork. In line with this, it has been reported that a block

356 in lagging strand replication does not result in fork arrest *in vitro*, but rather is bypassed via
357 re-priming by Polα/Primase allowing the fork to progress [52]. One potential explanation for
358 our findings is that the stabilisation of G4 structures via PDS treatment has also been shown
359 to result in a further potential barrier to replication fork processivity in the form of R-loops,
360 with both PDS-mediated DNA damage and micronuclei formation abrogated upon the
361 overexpression of RNase H1 [53]. Consistent with an important role for R-loops in facilitating
362 ALT, overexpression of RNase H1 in ALT cells has been shown to abrogate ALT markers,
363 whereas the loss of RNase H1 or FANCM (a factor also linked to the prevention of R-loop
364 formation), have the opposite effect [10–13].
365
366 Recent work has also suggested that PDS induced cytotoxicity is dependent on TOP2 [54],
367 inferring that the formation of G4 and/or R-loop structures leads to trapping of
368 topoisomerases which, in turn, may block replication fork progression [55]. We show here that,
369 analogous to PDS, treatment with the TOP2 poison ETO elicited markers of ALT specifically in
370 ATRX deplete cells. We note the largest induction of ALT markers manifested following
371 treatment with the TOP1 inhibitor CPT. Interestingly, poisoning of TOP1 by camptothecins
372 also effectively leads to the formation of R-loops [56,57]. We show here that the induction of C-
373 circles in ATRX null cells upon CPT treatment is most pronounced in the HeLa LT cell line,
374 which harbours very long telomeres of ~20 kb in length. This is consistent with previous
375 findings that the induction of ALT was most robust in this cell line upon co-depletion of ASF1a
376 and ASF1b [58]. The most likely explanation for this is that longer telomeres inherently provide
377 more opportunity for aberrant structures and/or genotoxic lesions to form. Indeed, each
378 telomeric repeat has been shown to represent a potential TOP1 cleavage site [59].
379

Strikingly, we further report here that the combined depletion of ATRX and the histone H3 K36me3 methyltransferase SETD2 triggers a dramatic induction of ALT pathway markers, akin to that observed upon CPT treatment. Mutations in SETD2 have been identified in ~15% of paediatric HGGs and are highly coincident with ATRX loss [45]. Here, we report that depletion of SETD2 leads to an enrichment of R-loops at telomeres, which in turn facilitates the ALT pathway in the absence of ATRX. This raises the interesting question as to how SETD2 normally modulates the formation of telomeric R-loops? Histone H3 K36me3 is known to recruit a variety of chromatin associated proteins, many with defined roles in reshaping chromatin accessibility following transcription, including MRG15 (a component of the Rpd3S/Sin3S histone deacetylase complex) [60], SPT16 (a component of the FACT complex) [61] and PHF1/19 (a component of the polycomb repressive complex 2 (PRC2)) [62,63]. One possibility therefore is that a more open telomeric chromatin structure upon SETD2 loss is more permissive to the formation of R-loop and/or G-loop structures. In line with this hypothesis, loss of FACT has previously been linked to increases in R-loop formation [64]. Histone H3 K36me3 has also been shown to recruit the DNA methyltransferase DNMT3b, loss of which has been shown to induce hypomethylation at sub-telomeres and the accumulation of telomeric R-loops in patients with ICF (Immunodeficiency, Centromeric instability and Facial anomalies) syndrome [65]. Taken together, the data we present here suggests that it is the combination of increased telomeric R-loops upon SETD2 disruption, in concert with ATRX loss, that triggers the ALT pathway in this cohort of paediatric HGG.

Mutations in histone H3.3 at glycine 34 to arginine or valine (G34R/V) are also highly co-incident with ATRX loss in HGG and tend to be mutually exclusive with SETD2 mutations [16,45]. Indeed, these mutations are thought to impede the ability of SETD2 to methylate the H3 tail,

suggesting that in all likelihood the mechanism of ALT induction in tumours with this mutational signature phenocopies that of a SETD2 mutant, with the accumulation of telomeric R-loops. H3.3 G34R/V has, however, only been shown to obstruct SETD2 activity in *cis* [66,67] and this conjecture is therefore dependent on the mutant histone being incorporated into telomeric chromatin. In support of this possibility, recent work has shown that in the absence ATRX/DAXX, the histone H3.3 chaperone HIRA is enriched at ALT telomeres as an adaptive response to allow the deposition of histone H3.3 at telomeres [68]. A second mutation in histone H3.3 at lysine 27 to methionine (K27M) is also highly coincident with ATRX loss and inhibits the catalytic activity of PRC2 [16,45,67]. It will therefore be of interest to ascertain whether the inhibition of PRC2 also elicits ALT markers when combined with ATRX/DAXX loss and, if so, whether loss of PRC2 function leads to the accumulation of aberrant secondary structures on telomeric DNA.

ATRX has previously been implicated with multiple roles at the replication fork which could explain the data we present here, including roles in both the protection of stalled forks from nucleolytic degradation [28] and the restart of stalled replication forks [29,32]. Of note, ATRX has been proposed to interact with factors known to modulate both fork restart and protection. ATRX has been shown to interact and cooperate with FANCD2 to recruit CtIP to stalled replication forks and promote MRE11 dependent fork restart. ATRX itself has also been shown to interact with components of the MRN complex, raising the intriguing possibility that ATRX constitutes a component of a fork restart complex [20,29,32]. Understanding how these interactions are regulated will likely give important insights as to how ATRX facilitates progressive DNA replication through genotoxic lesions and/or aberrant DNA secondary structures.

A second implication of the data presented here is that ATRX/DAXX may have a direct role in the clearing or resolution of structures or genotoxic lesions on telomeric DNA. Of note, ATRX possesses a translocase activity [69] which could potentially resolve R-loops via branch migration. Indeed, loss of ATRX has been shown to lead to an increase in telomeric R-loops at a highly transcribed ectopic telomeric repeat [27], consistent with a role for ATRX in clearing R-loops once they have been triggered. R-loops have also been suggested to be excised by the nucleotide excision repair (NER) nucleases XPG and XPF, resulting in the formation of a single strand break, which could then ultimately trigger fork collapse in S-phase [70]. Interestingly, histone H3.3 deficient chicken DT40 cells have recently been shown to exhibit a likely defect in NER [71], raising the interesting possibility that ATRX/DAXX may be the histone H3.3 chaperone facilitating the completion of this process. In line with this notion, the nicking of telomeric DNA to form single stand breaks using the CRISPR-Cas9 system has been shown to induce the formation of C-circles in ATRX proficient cells [7].

Finally, we report that the KO of ATRX in HeLa LT cells is associated with a marked loss of telomere sister chromatid cohesion, consistent with a recent report in mouse cells, published during the preparation of this manuscript [49]. How ATRX normally maintains telomere cohesion remains an interesting question, nonetheless this observation likely accounts for the net gain in telomere length observed as a result of the BIR-like pathway in ALT cancer cells by facilitating the use of an out of register telomere template. Taken together, work presented here suggests that ATRX has a multi-faceted role in the suppression of the ALT pathway, accounting for its role as a near universal tumour suppressor in these cancers. Firstly, ATRX protects replication forks from collapse in the presence of telomeric lesions including R-loop structures. Secondly, ATRX maintains cohesion between sister telomeres, ensuring the

faithful use of BIR without aberrant increases in telomere length. Finally, we provide evidence that the induction of ALT requires two independent cellular events; the loss of ATRX/DAXX in conjunction with the loss of another factor or factors that lead to the formation of lesions or structures at telomeres, as exemplified here by SETD2 (Figure 7C).

ACKNOWLEDGEMENTS

We thank Prof. Amato Giaccia and Dr. Andrew Blackford for helpful discussions. HeLa LT cells were a kind gift from Dr. Roderick O'Sullivan. We acknowledge Kevin Clark in the MRC Weatherall Institute of Molecular Medicine (WIMM) Flow Cytometry Facility for providing cell-sorting services and technical expertise; Dominic Waithe and Christoffer Lagerholm in the Wolfson Imaging Centre for help with microscopy and data analysis; Philip Hublitz in MRC WIMM Genome Engineering Facility for preparation of RNase H overexpression vectors; Ryan Beveridge in the MRC WIMM Virus Screening Facility for help in generation of lentiviral preparations. These facilities are supported by the MRC Molecular Hematology Unit (MC_UU_12009), the MRC Human Immunology Unit (MC_UU_12010), the Wolfson Foundation (grant 18272), the Wellcome Trust (Micron107457/Z/15Z), the National Institute for Health Research Oxford Biomedical Research Centre (IS-BRC-1215-20008), the Cancer Research UK (CRUK) Oxford Centre, the KayKendall Leukemia Fund (KKL1057), the John Fell Fund (131/030 and 101/517), the EPA fund (CF182 and CF170) and the MRC WIMM Strategic Alliance (G0902418 andMC_UU_12025). The Clynes laboratory is supported through a Children with Cancer UK Paul O' Gorman Career Development Fellowship (15-202). T.K. and T.G. are supported through MRC Studentships. S.S. is funded through CRUK OIRO

(C5255/A23755). S.K. is supported through a Kwanjeong Educational Foundation (KEF) PhD scholarship. S.C. is funded through MRC OIRO (MC_UU_00001).

AUTHOR CONTRIBUTIONS

This project was conceived and supervised by D.C. with support from R.J.G and T.H. T.G., T.K., S.S. and S.C. performed the majority of the experiments. S.K. performed all cell proliferation assays. D.C. wrote the manuscript. T.K. and T.G. prepared the figures. R.J.G, T.H, T.G., and T.K. critically reviewed the manuscript.

DECLARATION OF INTERESTS

The authors declare no competing interests.

ONLINE METHODS

Cell lines and cell culture conditions

Cell lines used are listed in Supplementary Table 2. All cell lines were obtained from ATCC with the exception of HeLa LT which was a kind gift from Roderick O'Sullivan [34] and HeLa ST (Hela H3.3-SNAP) were a kind gift from Genevieve Almouzni [72]. All cells were cultured in standard Dulbecco's Modified Eagle's Medium (DMEM) media supplemented with 10% foetal calf serum, 1% L-glutamine and 1% PenStrep (Gibco). U-2 OS^{ATRX} cells were cultured in the presence of 0.4 µg/mL puromycin and 175 µg/mL neomycin. Ectopic ATRX expression was driven through the addition of 0.4 µg/mL doxycycline.

CRISPR-Cas9 KO

CRISPR-Cas9 KO of ATRX was performed using a modified pSpCas9(bb)-2A-GFP tagged Cas9 vector containing sgRNAs targeting exon 16 of ATRX (sgRNA sequence - TOP: 5' caccGTCCAATAACAACCA^AGT 3', BOTTOM: 5' aaacACT^TGGTTGTTATTGGAC 3') with an expected cut site at lysine 1536. Cells were sorted on a BD FACSAria Fusion cell sorter 24 hours after transfection into single wells and grown into clones. KO was determined by western blotting. DAXX KOs were performed using a commercially available DAXX Cas9 plasmid (Santa Cruz, sc-400686-KO-2) and were FACs sorted based on GFP expression. SETD2 Cas9 KO was performed as described in [73]. Transfected cells were selected using 0.4 µg/mL puromycin and then sorted into single wells to obtain clones. Combinatorial KOs were made through sequential KO of genes.

Treatment of Cells with Genotoxic Agents

Cells were treated with these genotoxic agents at the following doses for 48 hours prior to downstream analysis with the ALT assays used in this study: PDS at 5 μM, CPT at 50 nM, APH at 0.2 μM and ETO at 0.5 μM.

siRNA Knockdown

Mus81 siRNA experiments were performed using the commercially available ON-TARGETplus Mus81 siRNA SmartPool (Dharmacon, L-016143-01-0005). Cells were reverse transfected when seeding cells to wells or coverslips using Lipofectamine RNAiMAX, to a final concentration of 5 pmol following the manufacturer's instructions. 48 hours after transfection well were forward transfected again to ensure consistent knockdown. For Mus81 experiments, 72 hours after transfection cells were treated with 5 μM PDS and incubated for a further 24 hours before harvesting.

ImmunoFISH

ImmunoFISH experiments were performed with cells seeded onto 13mm #00 thickness coverslips. Briefly, cells were pre-permeabilised with 0.5% Triton-X100 for 1 minute on ice then fixed in 4% paraformaldehyde for 20 minutes. Fixed coverslips were washed in PBS then permeabilised on ice for 6 minutes with 0.5% Triton-X100. Coverslips were blocked in blocking buffer (2% BSA, 0.1% Tween-20 in PBS) for 1 hour and then incubated with the appropriate primary antibody in blocking buffer. Following primary antibody staining, coverslips were

washed in PBST (0.5% Tween-20 in PBS) and stained with an appropriate Alexa fluorophore-conjugated secondary antibody. Following further washing, coverslips were post-fixed with 4% PFA for 20 minutes and then a Cy3-$[CCCTTA]_5$ probe was hybridised onto the coverslip in hybridisation buffer (25% formamide, 2xSSC, 200 ng/µL Salmon sperm, 5x Denhardts solution, 50 mM phosphase buffer, 1mM EDTA in water) overnight at 37°C in a humidified chamber. In instances where denatured telomere signals were required, coverslips were incubated in 3.5 N HCl for 13 minutes, then immediately washed with ice cold PBS prior to hybridisation with telomere probes. For analysis of single stranded telomeric DNA the denaturation step was omitted. Coverslips were then washed in 2x SSC before being mounted in VectaShield containing DAPI. Coverslips were then visualised using a DeltaVision widefield microscope.

C-circle Assay

DNA was extracted from approximately $1x10^6$ cells using the QIAGEN Core B kit. Extracted DNA was resuspended in 20 mM Tris-HCl. DNA was quantified and then 30 ng of genomic DNA was amplified in a PCR reaction containing ϕ29 polymerase, 1% Tween-20, 200 µg/mL BSA and dTTP, dGTP, and dATP, but lacking dCTP for 8 hours at 30°C followed by 20 minutes at 65°C. PCR reactions were run with and without ϕ29 polymerase to ensure the signal was specific for rolling-circle amplification products. Amplified samples were then blotted onto Zeta-Probe membrane (Bio-Rad) using a slot blotter.

Following fixing of DNA to the membrane with a UVA Stratalinker 2400, membranes were soaked in PerfectHyb Plus (Sigma Aldrich) for 20 minutes at room temperature. A 3' Digitonin (DIG) tagged $[CCCATT]_5$ oligonucleotide was then diluted in PerfectHyb to a final

562 concentration of 40 nM in 20mL hybridisation buffer, and was allowed to hybridise with the
563 membrane in a rolling incubator for 2 hours at 37°C. Following hybridisation, membranes
564 were briefly washed twice with wash buffer (0.1M Maleic acid, 3M NaCl; 0.1% Tween 20
565 adjusted to pH 7.5), before blocking for 30 minutes and probing with a DIG antibody for 30
566 minutes. Finally, membranes were vigorously washed 3 times with wash buffer before placing
567 into a cassette with CDP-Star solution. Blots were then developed onto Amersham Hyperfilm
568 ECL film.
569
570 *Terminal Restriction Fragment (TRF) assay*
571
572 Terminal restriction fragment assays were performed by first extracting genomic DNA as
573 described above with the QIAGEN Core B kit. Extracted DNA was quantified and at least 2 µg
574 of genomic DNA was digested overnight at 37°C with HinfI and RsaI restriction endonucleases.
575 Following digestion, samples were run on 0.8% agarose gels in 1x TAE at 60 V overnight. Gels
576 were denatured using 1M NaOH and then neutralised and blotted onto Zeta-Probe
577 membrane by upward capillary transfer. Blots were then probed with a DIG-tagged telomere
578 probe as described above. The blots were analysed and quantified using TeloMetric software
579 [74].
580
581 *Monochrome multiplex qPCR (mm-qPCR)*
582
583 MM-qPCR was carried out as described in [75] with some alterations. Genomic DNA samples
584 were diluted to 5 ng/µL. Primer sets are listed in Supplementary Table 3. Five concentrations
585 of reference genomic DNA purified from HeLa LT were prepared by 3-fold serial dilution (from

150 ng to 1.85 ng) to generate standard curves for relative quantitation of T/S ratios. For each sample, 20 ng of genomic DNA was mixed with 0.75× PowerUp SYBR Green Master Mix (Thermo Scientific), the primers (300 nM), and water to a final volume of 20 µL per well and analysed using a Thermo Fisher QuantStudio 3 qPCR machine with the following cycle conditions: denaturation for 15 min at 95 °C, followed by two cycles of 15 s at 94 °C/15 s at 49 °C and 32 cycles of 15 s at 94 °C/10 s at 62 °C/15 s at 74 °C with signal acquisition and 10 s at 84 °C/15 s at 88 °C with signal acquisition. Samples were run in triplicate, and analysis was repeated six times using independent runs.

Cohesion FISH

Cohesion FISH was performed using commercially available FISH probe set from Cytocell designed to detect DLEU7 deletion (Cytocell, LPH-043-S) following the manufacturers protocol. Coverslips were then visualised using a DeltaVision widefield microscope.

S9.6 DNA-RNA Immunoprecipitation (DRIP)

R-loop DRIP experiments were performed using the S9.6 antibody as described in [27]. Eluted DNA was analysed by slot blotting and probing using a DIG-tagged telomere probe as described above.

CellTiterGlo Assay

HeLa-LT cells were seeded on opaque 96-well plate at 100-500 cells in 100 µl of culture media per well. After 6-24 hours, an equal volume of the drug-containing media was added at the desired final concentrations. HU and APH treatment was performed for 72 hours and PDS treatment was performed for 7 days. The cell proliferation was assessed using CellTiter-Glo 2.0 Reagent (ProMega) according to the manufacturer's instructions. Briefly, the plate and the reagent were equilibrated at room temperature for 5 minutes, the media was removed from the plate, and 100 µl of the diluted reagent (1:5 in PBS) was added to each well. After 10 minutes, the plate was read via the ProMega GloMax Luminometer to assess the quantity of metabolically active cells. The IC50 values were derived by fitting the dose-response data into the curves via GraphPad Prism v8.0.

Triptolide Treatment and Cell Cycle Analysis by PI Staining

ATRX/SETD2 double KO cells were treated with increasing doses of the transcription inhibitor triptolide (25 nM, 50 nM and 100 nM) for 24 hours. gDNA was then extracted and the C-circle assay was performed as described above. To ensure cells were still progressing through the cell cycle, PI staining was utilised. Briefly, cells were harvested, washed in 1x PBS and fixed in 70% ethanol on ice for 30 minutes. Cells were washed again in PBS, treated with 100 µg/ml RNase A and then incubated with 50 µg/ml propidium iodide solution for 10 minutes at room temperature. Samples were then analysed by flow cytometry to estimate the percentage of cells in G1, S and G2 phases of the cell cycle.

RNase H Overexpression

Lentivirus-based constructs for overexpression of wildtype RNase H and the catalytically dead D210N mutant in HeLa cells were generated using InFusion cloning to insert the NLS-RNaseH-V5 sequences from plasmids ppCAG_RNaseH1_WT (Addgene #111906) and ppCAG_RNaseH1_D210N (Addgene #111904) into the pLeGO-C2 backbone (Addgene #27339). The ATRX/SETD2 double KO cells were transduced with the lentivirus and left for 14 days before DNA was harvested and C-circle analysis was carried out as described above. Efficient overexpression was assessed by Western blot.

Quantification and Statistical Analysis

Each experiment was repeated at least twice, with representative results shown. Statistical analysis was done using GraphPad Prism 9 (GraphPad Software Inc.). Unpaired t tests were used to compare two groups. One-way ANOVA was used to compare more than two groups. Sample sizes and p-values are shown in the figure legends. In all cases ns indicates $p > 0.05$.

652 **REFERENCES**

653 1. de Lange, T. Shelterin-Mediated Telomere Protection. (2018) doi:10.1146/annurev-
654 genet-032918.

655 2. Heaphy, C. M. *et al.* Prevalence of the alternative lengthening of telomeres telomere
656 maintenance mechanism in human cancer subtypes. *American Journal of Pathology*
657 **179**, 1608–1615 (2011).

658 3. Dilley, R. L. *et al.* Break-induced telomere synthesis underlies alternative telomere
659 maintenance. *Nature* **539**, 54–58 (2016).

660 4. Min, J., Wright, W. E. & Shay, J. W. Alternative Lengthening of Telomeres Mediated by
661 Mitotic DNA Synthesis Engages Break-Induced Replication Processes. (2017)
662 doi:10.1128/MCB.

663 5. Roumelioti, F. *et al.* Alternative lengthening of human telomeres is a conservative DNA
664 replication process with features of break-induced replication . *EMBO reports* **17**,
665 1731–1737 (2016).

666 6. Cho, N. W., Dilley, R. L., Lampson, M. A. & Greenberg, R. A. Interchromosomal
667 homology searches drive directional ALT telomere movement and synapsis. *Cell* **159**,
668 108–121 (2014).

669 7. Zhang, T. *et al.* Strand break-induced replication fork collapse leads to C-circles, C-
670 overhangs and telomeric recombination. *PLoS Genetics* **15**, (2019).

671 8. Sfeir, A. *et al.* Mammalian Telomeres Resemble Fragile Sites and Require TRF1 for
672 Efficient Replication. *Cell* **138**, 90–103 (2009).

673 9. Aguilera, A. & García-Muse, T. R Loops: From Transcription Byproducts to Threats to
674 Genome Stability. *Molecular Cell* vol. 46 115–124 (2012).

10. Silva, B. *et al.* FANCM limits ALT activity by restricting telomeric replication stress induced by deregulated BLM and R-loops. *Nature Communications* **10**, (2019).

11. Pan, X. *et al.* FANCM suppresses DNA replication stress at ALT telomeres by disrupting TERRA R-loops. *Scientific Reports* **9**, (2019).

12. Lu, R. *et al.* The FANCM-BLM-TOP3A-RMI complex suppresses alternative lengthening of telomeres (ALT). *Nature Communications* **10**, (2019).

13. Arora, R. *et al.* RNaseH1 regulates TERRA-telomeric DNA hybrids and telomere maintenance in ALT tumour cells. *Nature Communications* **5**, (2014).

14. Pan, X. *et al.* FANCM, BRCA1, and BLM cooperatively resolve the replication stress at the ALT telomeres. *Proceedings of the National Academy of Sciences of the United States of America* **114**, E5940–E5949 (2017).

15. Lovejoy, C. A. *et al.* Loss of ATRX, genome instability, and an altered DNA damage response are hallmarks of the alternative lengthening of Telomeres pathway. *PLoS Genetics* **8**, (2012).

16. Schwartzentruber, J. *et al.* Driver mutations in histone H3.3 and chromatin remodelling genes in paediatric glioblastoma. *Nature* **482**, 226–231 (2012).

17. Napier, C. E. *et al. ATRX represses alternative lengthening of telomeres*. *Oncotarget* vol. 6 www.impactjournals.com/oncotarget/ (2015).

18. Clynes, D. *et al.* Suppression of the alternative lengthening of telomere pathway by the chromatin remodelling factor ATRX. *Nature Communications* **6**, (2015).

19. Eid, R. *et al.* Genetic Inactivation of ATRX Leads to a Decrease in the Amount of Telomeric Cohesin and Level of Telomere Transcription in Human Glioma Cells . *Molecular and Cellular Biology* **35**, 2818–2830 (2015).

20. Clynes, D. *et al.* ATRX dysfunction induces replication defects in primary mouse cells. *PLoS ONE* **9**, (2014).

21. Brosnan-Cashman, J. A. *et al.* ATRX loss induces multiple hallmarks of the alternative lengthening of telomeres (ALT) phenotype in human glioma cell lines in a cell line-specific manner. *PLoS ONE* **13**, (2018).

22. Clynes, D., Higgs, D. R. & Gibbons, R. J. The chromatin remodeller ATRX: A repeat offender in human disease. *Trends in Biochemical Sciences* vol. 38 461–466 (2013).

23. Drané, P., Ouararhni, K., Depaux, A., Shuaib, M. & Hamiche, A. The death-associated protein DAXX is a novel histone chaperone involved in the replication-independent deposition of H3.3. *Genes and Development* **24**, 1253–1265 (2010).

24. Goldberg, A. D. *et al.* Distinct Factors Control Histone Variant H3.3 Localization at Specific Genomic Regions. *Cell* **140**, 678–691 (2010).

25. Wong, L. H. *et al.* ATRX interacts with H3.3 in maintaining telomere structural integrity in pluripotent embryonic stem cells. *Genome Research* **20**, 351–360 (2010).

26. Wang, Y. *et al.* G-quadruplex DNA drives genomic instability and represents a targetable molecular abnormality in ATRX-deficient malignant glioma. *G-quadruplex DNA drives genomic instability and represents a targetable molecular abnormality in ATRX-deficient malignant glioma* 347542 (2018) doi:10.1101/347542.

27. Nguyen, D. T. *et al.* The chromatin remodelling factor ATRX suppresses R-loops in transcribed telomeric repeats . *EMBO reports* **18**, 914–928 (2017).

28. Huh, M. S. *et al.* Stalled replication forks within heterochromatin require ATRX for protection. *Cell Death and Disease* **7**, (2016).

29. Leung, J. W. C. *et al.* Alpha thalassemia/mental retardation syndrome X-linked gene product ATRX is required for proper replication restart and cellular resistance to replication stress. *Journal of Biological Chemistry* **288**, 6342–6350 (2013).

30. Watson, L. A. *et al.* Atrx deficiency induces telomere dysfunction, endocrine defects, and reduced life span. *Journal of Clinical Investigation* **123**, 2049–2063 (2013).

31. Juhász, S., Elbakry, A., Mathes, A. & Löbrich, M. ATRX Promotes DNA Repair Synthesis and Sister Chromatid Exchange during Homologous Recombination. *Molecular Cell* **71**, 11-24.e7 (2018).

32. Raghunandan, M. *et al.* Functional cross talk between the Fanconi anemia and ATRX/DAXX histone chaperone pathways promotes replication fork recovery. *Human molecular genetics* **29**, 1083–1095 (2020).

33. Koschmann, C. *et al.* C A N C E R ATRX loss promotes tumor growth and impairs nonhomologous end joining DNA repair in glioma. *Science Translational Medicine* **8**, undefined (2016).

34. O'Sullivan, R. J. *et al.* Rapid induction of alternative lengthening of telomeres by depletion of the histone chaperone ASF1. *Nature Structural and Molecular Biology* **21**, 167–174 (2014).

35. Spiegel, J., Adhikari, S. & Balasubramanian, S. The Structure and Function of DNA G-Quadruplexes. *Trends in Chemistry* vol. 2 123–136 (2020).

36. Law, M. J. *et al.* ATR-X syndrome protein targets tandem repeats and influences allele-specific expression in a size-dependent manner. *Cell* **143**, 367–378 (2010).

37. Loe, T. K. *et al.* Telomere length heterogeneity in ALT cells is maintained by PML-dependent localization of the BTR complex to telomeres. *Genes and Development* **34**, 650–662 (2020).

744 38. Bryan, T. M., Englezou, A., Gupta, J., Bacchetti, S. & Reddel, R. R. Telomere elongation
745 in immortal human cells without detectable telomerase activity. *EMBO Journal* **14**,
746 4240–4248 (1995).
747 39. Bakkenist, C. J. & Kastan, M. B. *DNA damage activates ATM through intermolecular*
748 *autophosphorylation and dimer dissociation*. www.nature.com/nature (2003).
749 40. Pepe, A. & West, S. C. MUS81-EME2 promotes replication fork restart. *Cell Reports* **7**,
750 (2014).
751 41. Zeng, S. *et al.* Telomere recombination requires the MUS81 endonuclease. *Nature Cell*
752 *Biology* **11**, 616–623 (2009).
753 42. Zellweger, R. *et al.* Rad51-mediated replication fork reversal is a global response to
754 genotoxic treatments in human cells. *Journal of Cell Biology* **208**, 563–579 (2015).
755 43. Ray Chaudhuri, A. *et al.* Topoisomerase i poisoning results in PARP-mediated
756 replication fork reversal. *Nature Structural and Molecular Biology* **19**, 417–423 (2012).
757 44. Udugama, M. *et al.* Ribosomal DNA copy loss and repeat instability in ATRX-mutated
758 cancers. *Proceedings of the National Academy of Sciences of the United States of*
759 *America* **115**, 4737–4742 (2018).
760 45. Fontebasso, A. M. *et al.* Mutations in SETD2 and genes affecting histone H3K36
761 methylation target hemispheric high-grade gliomas. *Acta Neuropathologica* **125**, 659–
762 669 (2013).
763 46. Kanu, N. *et al.* SETD2 loss-of-function promotes renal cancer branched evolution
764 through replication stress and impaired DNA repair. *Oncogene* **34**, 5699–5708 (2015).
765 47. Pan, X. *et al.* FANCM, BRCA1, and BLM cooperatively resolve the replication stress at
766 the ALT telomeres. *Proceedings of the National Academy of Sciences of the United*
767 *States of America* **114**, E5940–E5949 (2017).

768 48. Yang, Z., Takai, K. K., Lovejoy, C. A. & de Lange, T. Break-induced replication promotes
769 fragile telomere formation. *Genes & Development* (2020)
770 doi:10.1101/gad.328575.119.
771 49. Lovejoy, C. A., Takai, K., Huh, M. S., Picketts, D. J. & de Lange, T. ATRX affects the repair
772 of telomeric DSBs by promoting cohesion and a DAXX-dependent activity. *PLoS biology*
773 **18**, e3000594 (2020).
774 50. Graham, M. K. *et al.* Functional loss of ATRX and TERC activates Alternative
775 Lengthening of Telomeres (ALT) in LAPC4 prostate cancer cells. *Molecular Cancer*
776 *Research* **17**, 2480–2491 (2019).
777 51. Huh, M. S. *et al.* Compromised genomic integrity impedes muscle growth after Atrx
778 inactivation. *Journal of Clinical Investigation* **122**, 4412–4423 (2012).
779 52. Taylor, M. R. G. & Yeeles, J. T. P. The Initial Response of a Eukaryotic Replisome to DNA
780 Damage. *Molecular Cell* **70**, 1067-1080.e12 (2018).
781 53. de Magis, A. *et al.* DNA damage and genome instability by G-quadruplex ligands are
782 mediated by R loops in human cancer cells. *Proceedings of the National Academy of*
783 *Sciences of the United States of America* **116**, 816–825 (2019).
784 54. Olivieri, M. *et al.* A Genetic Map of the Response to DNA Damage in Human Cells. *Cell*
785 **182**, 481-496.e21 (2020).
786 55. Tammaro, M., Barr, P., Ricci, B. & Yan, H. Replication-dependent and transcription-
787 dependent mechanisms of DNA double-strand break induction by the topoisomerase
788 2-targeting drug etoposide. *PLoS ONE* **8**, (2013).
789 56. Sordet, O. *et al.* Ataxia telangiectasia mutated activation by transcription- and
790 topoisomerase I-induced DNA double-strand breaks. *EMBO Reports* **10**, 887–893
791 (2009).

57. Marinello, J., Chillemi, G., Bueno, S., Manzo, S. G. & Capranico, G. Antisense transcripts enhanced by camptothecin at divergent CpG-island promoters associated with bursts of topoisomerase I-DNA cleavage complex and R-loop formation. *Nucleic Acids Research* **41**, 10110–10123 (2013).

58. O'Sullivan, R. J. *et al.* Rapid induction of alternative lengthening of telomeres by depletion of the histone chaperone ASF1. *Nature Structural and Molecular Biology* **21**, 167–174 (2014).

59. Kang, M. R., Muller, M. T. & Chung, I. K. Telomeric DNA damage by topoisomerase I: A possible mechanism for cell killing by camptothecin. *Journal of Biological Chemistry* **279**, 12535–12541 (2004).

60. Kumar, G. S. *et al.* Sequence requirements for combinatorial recognition of histone H3 by the MRG15 and Pf1 subunits of the Rpd3S/Sin3S corepressor complex. *Journal of Molecular Biology* **422**, 519–531 (2012).

61. Carvalho, S. *et al.* Histone methyltransferase SETD2 coordinates FACT recruitment with nucleosome dynamics during transcription. *Nucleic Acids Research* **41**, 2881–2893 (2013).

62. Ballaré, C. *et al.* Phf19 links methylated Lys36 of histone H3 to regulation of Polycomb activity. *Nature Structural and Molecular Biology* **19**, 1257–1265 (2012).

63. Cai, L. *et al.* An H3K36 Methylation-Engaging Tudor Motif of Polycomb-like Proteins Mediates PRC2 Complex Targeting. *Molecular Cell* **49**, 571–582 (2013).

64. Herrera-Moyano, E., Mergui, X., García-Rubio, M. L., Barroso, S. & Aguilera, A. The yeast and human FACT chromatinreorganizing complexes solve R-loopmediated transcription-replication conflicts. *Genes and Development* **28**, 735–748 (2014).

65. Sagie, S. *et al.* Telomeres in ICF syndrome cells are vulnerable to DNA damage due to elevated DNA:RNA hybrids. *Nature Communications* **8**, (2017).

66. Weinberg, D. N., Allis, C. D. & Lu, C. Oncogenic mechanisms of histone H3 mutations. *Cold Spring Harbor Perspectives in Medicine* vol. 7 (2017).

67. Lewis, P. W. *et al.* Inhibition of PRC2 activity by a gain-of-function H3 mutation found in pediatric glioblastoma. *Science* **340**, 857–861 (2013).

68. Hoang, S. M. *et al.* Regulation of ALT-associated homology-directed repair by polyADP-ribosylation. *Nature Structural and Molecular Biology* (2020) doi:10.1038/s41594-020-0512-7.

69. Xue, Y. *et al. The ATRX syndrome protein forms a chromatin-remodeling complex with Daxx and localizes in promyelocytic leukemia nuclear bodies*. vol. 100 www.pnas.orgcgidoi10.1073pnas.1937626100 (2003).

70. Sollier, J. *et al.* Transcription-Coupled Nucleotide Excision Repair Factors Promote R-Loop-Induced Genome Instability. *Molecular Cell* **56**, 777–785 (2014).

71. Frey, A., Listovsky, T., Guilbaud, G., Sarkies, P. & Sale, J. E. Histone H3.3 is required to maintain replication fork progression after UV damage. *Current Biology* **24**, 2195–2201 (2014).

72. Adam, S., Polo, S. E. & Almouzni, G. XTranscription recovery after DNA damage requires chromatin priming by the H3.3 histone chaperone HIRA. *Cell* **155**, 94 (2013).

73. Pfister, S. X. *et al.* Inhibiting WEE1 Selectively Kills Histone H3K36me3-Deficient Cancers by dNTP Starvation. *Cancer Cell* **28**, 557–568 (2015).

74. Grant, J. D. *et al.* Telometric: A Tool Providing Simplified, Reproducible Measurements of Telomeric DNA from Constant Field Agarose Gels. *BioTechniques* **31**, 1314–1318 (2001).

75. Cawthon, R. M. Telomere length measurement by a novel monochrome multiplex quantitative PCR method. *Nucleic Acids Research* **37**, (2009).

FIGURE LEGENDS

Figure 1. Loss of ATRX alone is insufficient to trigger the ALT pathway. A) Immunoblot confirming CRISPR-Cas9 mediated KO of ATRX in two independent clones of HeLa LT. B-C) C-circle blot and quantification showing that deletion of ATRX in the HeLa LT cell line is insufficient to trigger the accumulation of C-circles, n=3. – Phi 29 is a negative control performed without the addition of the phi29 polymerase. U-2 OS is included as an ALT-positive positive control. D-E) ImmunoFISH detection of ALT associated PML Nuclear Bodies (APBs) both in the presence and absence of ATRX, showing no induction of APB formation upon ATRX loss, >200 nuclei analysed across 3 biological replicates. F) Terminal Restriction Fragment (TRF) analysis of telomere length showing no overt changes in telomere length or heterogeneity upon ATRX deletion. In all panels, ns signifies $p > 0.05$, determined by one-way ANOVA.

Figure 2. Treatment with PDS in combination with ATRX loss triggers ALT markers. A-B) C-circle blot and quantification showing C-circle accumulation specifically in ATRX KO clones following 48 hrs treatment with 5µM PDS, n=3. ****$p < 0.0001$ determined by one-way ANOVA. C-D) Representative images and quantification of APB induction in HeLa LT ATRX KO clones upon 48 hrs treatment with 5µM PDS, >200 nuclei analysed across 3 biological replicates. **$p < 0.001$, ****$p < 0.0001$, determined by one-way ANOVA. E-F) Representative images and quantification of RPA ssTel in HeLa LT ATRX KO upon treatment with 48 hrs 5µM PDS, >150 nuclei analysed across 3 biological replicates. **$p < 0.001$, ****$p < 0.0001$, determined by one-way ANOVA. G) TRF analysis showing treatment with 5µM PDS for 48 hrs increased telomere length heterogeneity specifically upon depletion of ATRX. Telomere

heterogeneity was measured using Telometric software, n=2. *p < 0.05, determined by one-way ANOVA.

Figure 3. PDS induced ALT markers require replication fork collapse. A-B) Representative figure and quantification of pATM induction at telomeres upon PDS treatment. >150 nuclei analysed across 3 biological replicates. **p < 0.001, ***p < 0.0001, ****p < 0.0001, determined by one-way ANOVA. C) Immunoblot showing siRNA mediated knockdown of Mus81 in ATRX WT and ATRX KO cells. D) C-circle quantification showing induction of C-circles upon ATRX loss and PDS treatment is dependent on Mus81, n=3. *p < 0.05, **p < 0.001, determined by one-way ANOVA. E-F) Representative images and quantification from ImmunoFISH data showing the induction of RPA ssTel foci upon ATRX loss and PDS treatment is dependent on Mus81, >150 nuclei analysed across 3 biological replicates. ****p < 0.0001, determined by one-way ANOVA.

Figure 4. A variety of genotoxic agents induce markers of ALT in ATRX deficient cells. ALT markers for HeLa LT ATRX KO cells treated with low dose CPT, ETO and APH. A) C-circle blot and quantification, n=3. *p < 0.05, **p < 0.001, ***p < 0.0001, ****p < 0.0001, determined by one-way ANOVA. B) Representative ImmunoFISH to detect APBs following treatment of ATRX KO cells with CPT, APH and ETO, >200 nuclei analysed across 3 biological replicates. C) Quantification of APBs in treated HeLa LT cells. ****p < 0.0001, determined by one-way ANOVA. D) Representative RPA ssTel immunoFISH images in HeLa LT ATRX KO cells treated with the same panel of genotoxic agents. E) Quantification of RPA ssTel foci, >150 nuclei analysed across 3 biological replicates. *p < 0.05, **p < 0.001, ****p < 0.0001, determined by one-way ANOVA.

Figure 5: ATRX and DAXX act epistatically in the suppression of induced ALT. A) Immunoblot of CRISPR-Cas9 mediated DAXX knockouts in HeLa LT ATRX WT and HeLa LT ATRXΔ1 cell lines. B-C) C-circle blot and quantification in DAXX KO clones following treatment with PDS and CPT, n=3. *p < 0.05, **p < 0.001, ***p < 0.0001, ****p < 0.0001, determined by one-way ANOVA. D-E) RPA ssTel representative images and quantification in DAXX KO clones following PDS treatment, >200 nuclei analysed across 3 biological replicates. p < 0.0001, ****p < 0.0001, determined by one-way ANOVA. F-G) Quantification of APBs following PDS or CPT treatment in ATRX/DAXX KO clones, >200 nuclei analysed across 3 biological replicates. **p < 0.001, ***p < 0.0001, ****p < 0.0001, determined by one-way ANOVA.

Figure 6. SETD2 loss in combination with ATRX loss triggers markers of the ALT pathway. A) Immunoblot showing loss of H3 K36me3 upon CRISPR-Cas9 mediated deletion of SETD2. B-C) C-circle blot and quantification showing accumulation of C-circles specifically upon co-deletion of both ATRX and SETD2 in HeLa LT cells, n=3. **p < 0.001, ***p < 0.0001, determined by one-way ANOVA. D) APB analysis showing accumulation of APBs specifically upon co-depletion of ATRX and SETD2, >100 nuclei analysed across 3 biological replicates. **p < 0.001, determined by one-way ANOVA. E) Quantification of RPA ssTel positive telomeres upon co-depletion of ATRX and SETD2, >150 nuclei analysed across 2 biological replicates. ****p < 0.0001, determined by one-way ANOVA. F) Immunoblot showing combined loss of ATRX and SETD2 leads to DNA damage. G) C-circle assay quantification in ATRX/SETD knockout cells treated with triptolide at indicated concentrations, n=2. *p < 0.05, **p < 0.001, ***p < 0.0001, determined by one-way ANOVA. H) S9.6 DRIP slot blot and quantification showing increased levels of R loops at telomeres upon SETD2 loss, n=3. **p < 0.001, determined by unpaired

Student's t test. I) Immunoblot showing overexpression of RNase H WT and the catalytically dead D210N mutant in the HeLa LT ATRX/SETD2Δ1 14 days after lentiviral transduction. J) S9.6 DRIP slot blot and quantification showing loss of telomeric R-loops upon ectopic expression of RNase H WT but not the D210N mutant, n=2. K) C-circle blot and quantification of ATRX/SETD2Δ1 cells overexpressing RNase H WT or the D210N mutant 14 days following transfection, n=3. **p < 0.001, determined by unpaired Student's t test.

Figure 7. Loss of ATRX induces loss of telomere sister chromatid cohesion. A) FISH of 156 kb region of chromosome 13 covering the D3S319-del genetic marker (red) and 13qter subtelomeric probe (green). Loss of sister chromatid cohesion is observed as a doublet, >50 nuclei analysed across 2 biological replicates. B) Quantification of doublet formation using the 13qter subtelomeric probe. *p < 0.05, ****p < 0.00001, determined by one-way ANOVA. C) Proposed model for suppression of the ALT pathway by the chromatin remodelling factor ATRX.

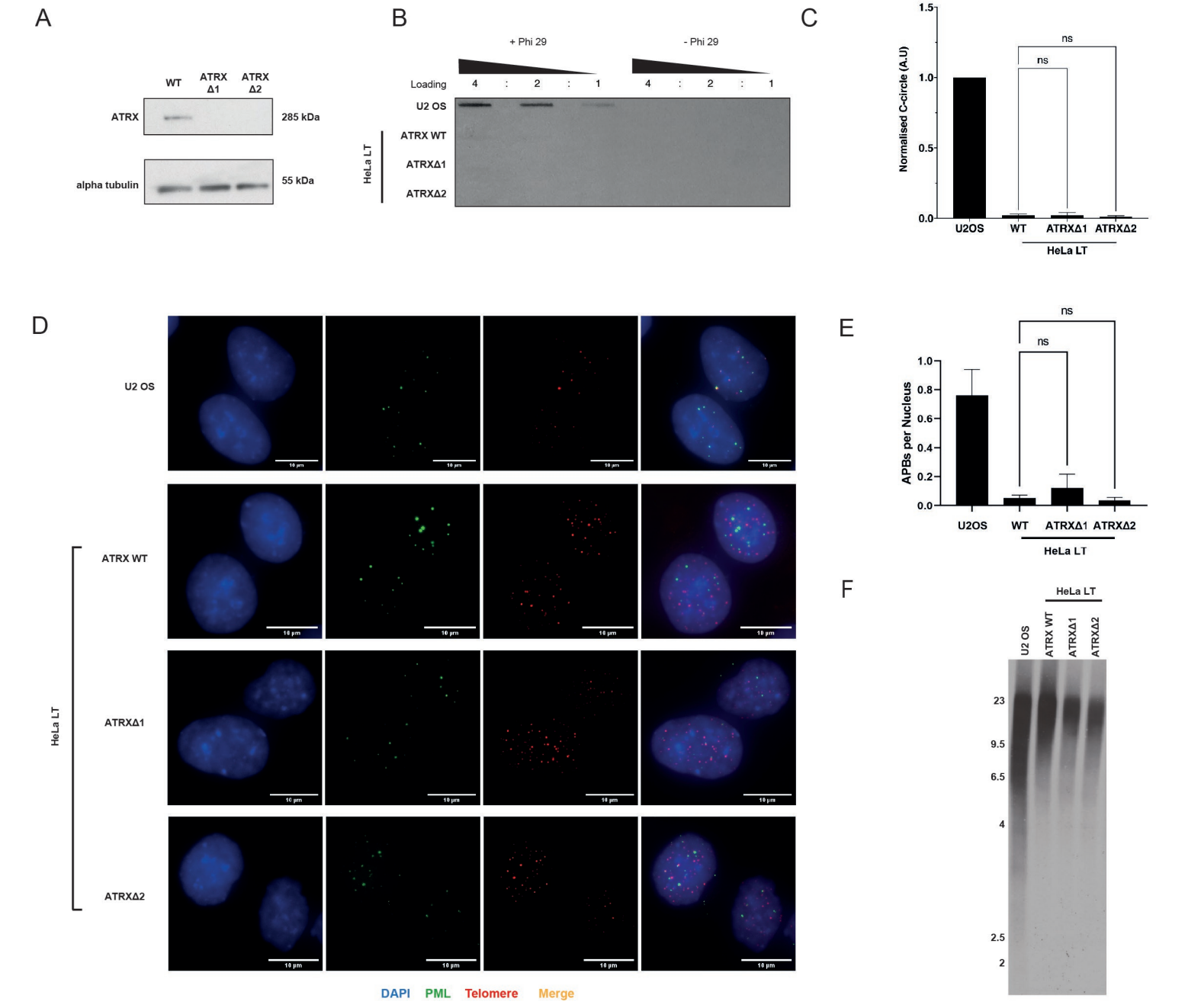
A
WT
ATRX Δ1
ATRX Δ2
ATRX
285 kDa
alpha tubulin
55 kDa
B
+ Phi 29
- Phi 29
Loading
4 : 2 : 1
4 : 2 : 1
U2 OS
HeLa LT
ATRX WT
ATRXΔ1
ATRXΔ2
C
Normalised C-circle (A.U)
1.5
1.0
0.5
0.0
ns
ns
U2OS
WT
ATRXΔ1
ATRXΔ2
HeLa LT
D
U2 OS
HeLa LT
ATRX WT
ATRXΔ1
ATRXΔ2
DAPI
PML
Telomere
Merge
E
APBs per Nucleus
1.0
0.8
0.6
0.4
0.2
0.0
ns
ns
U2OS
WT
ATRXΔ1
ATRXΔ2
HeLa LT
F
HeLa LT
U2 OS
ATRX WT
ATRXΔ1
ATRXΔ2
23
9.5
6.5
4
2.5
2

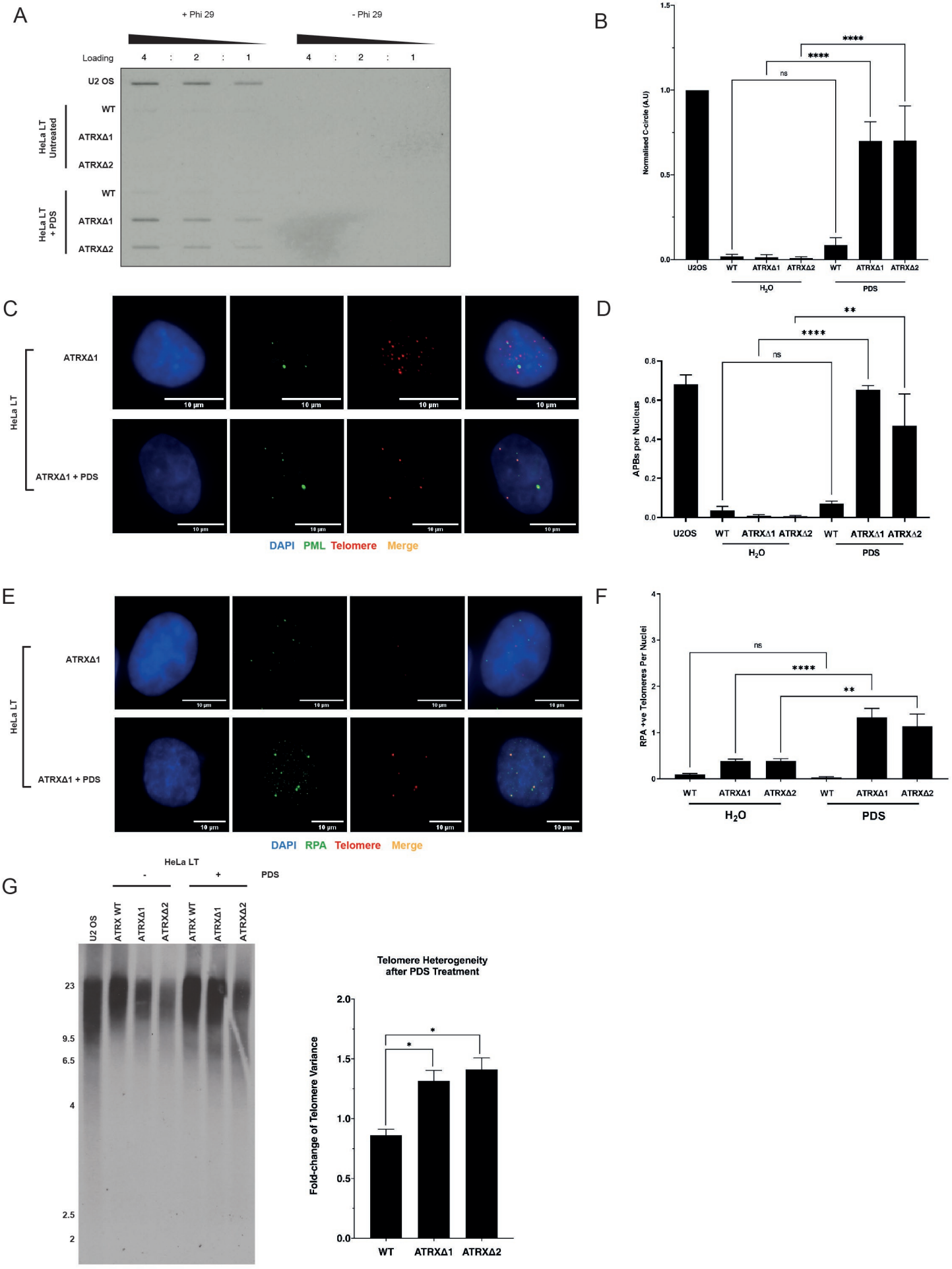
A
+ Phi 29
- Phi 29
Loading
4 : 2 : 1
4 : 2 : 1
U2 OS
HeLa LT Untreated
WT
ATRXΔ1
ATRXΔ2
HeLa LT + PDS
WT
ATRXΔ1
ATRXΔ2
B
Normalised C-circle (A.U)
1.5
1.0
0.5
0.0
****
****
ns
U2OS
WT
ATRXΔ1
ATRXΔ2
WT
ATRXΔ1
ATRXΔ2
H2O
PDS
C
HeLa LT
ATRXΔ1
ATRXΔ1 + PDS
10 μm
DAPI PML Telomere Merge
D
APBs per Nucleus
0.8
0.6
0.4
0.2
0.0
**
****
ns
U2OS
WT
ATRXΔ1
ATRXΔ2
WT
ATRXΔ1
ATRXΔ2
H2O
PDS
E
HeLa LT
ATRXΔ1
ATRXΔ1 + PDS
10 μm
DAPI RPA Telomere Merge
F
RPA +ve Telomeres Per Nuclei
4
3
2
1
0
ns
****
**
WT
ATRXΔ1
ATRXΔ2
WT
ATRXΔ1
ATRXΔ2
H2O
PDS
G
HeLa LT
-
+
PDS
U2 OS
ATRX WT
ATRXΔ1
ATRXΔ2
ATRX WT
ATRXΔ1
ATRXΔ2
23
9.5
6.5
4
2.5
2
Telomere Heterogeneity after PDS Treatment
Fold-change of Telomere Variance
2.0
1.5
1.0
0.5
0.0
*
*
WT
ATRXΔ1
ATRXΔ2

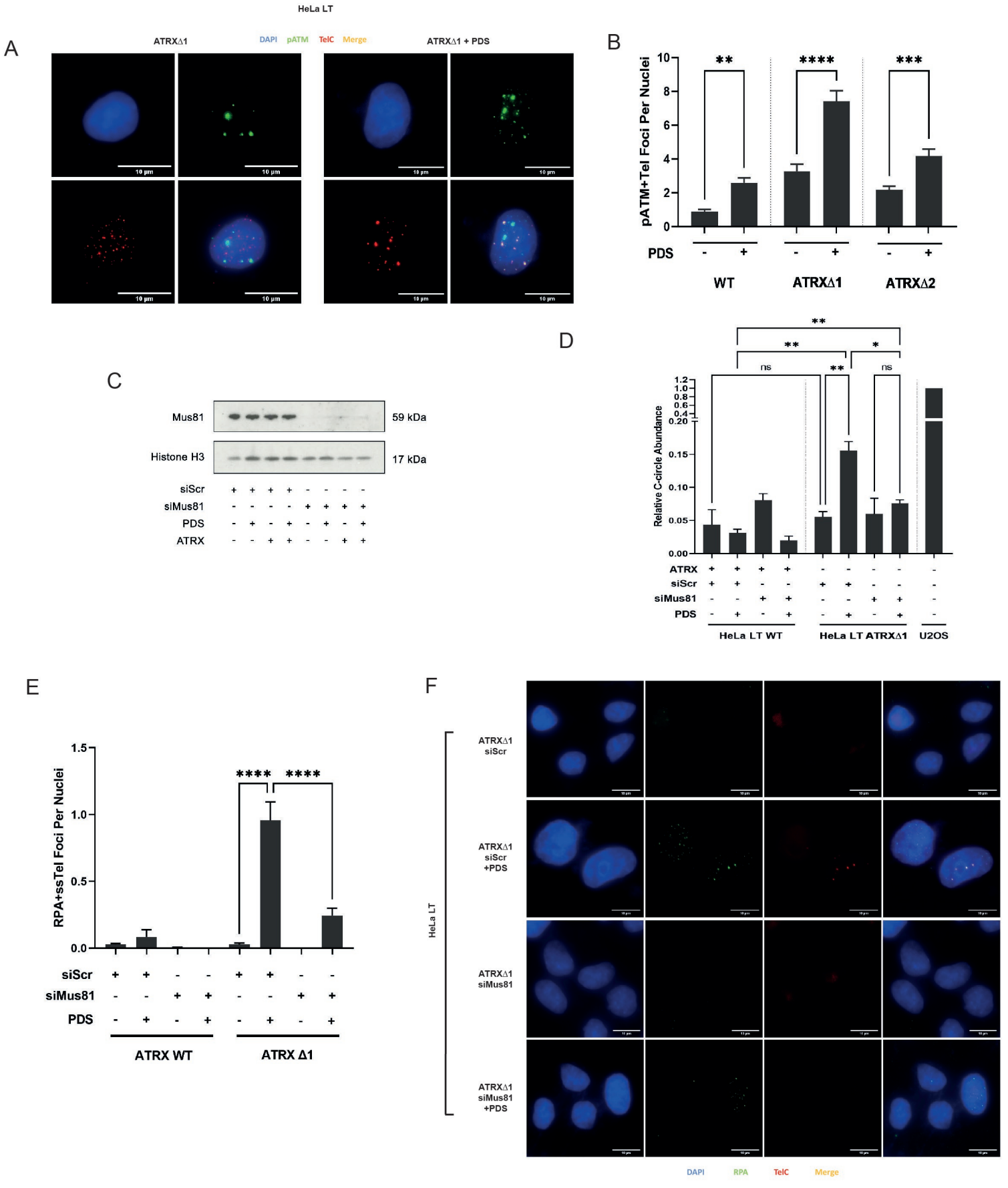
A
HeLa LT
ATRXΔ1
DAPI pATM TelC Merge
ATRXΔ1 + PDS
10 μm
B
pATM+Tel Foci Per Nuclei
**
****
***
PDS
WT
ATRXΔ1
ATRXΔ2
C
Mus81
59 kDa
Histone H3
17 kDa
siScr
siMus81
PDS
ATRX
D
Relative C-circle Abundance
ns
**
*
ATRX
siScr
siMus81
PDS
HeLa LT WT
HeLa LT ATRXΔ1
U2OS
E
RPA+ssTel Foci Per Nuclei
****
siScr
siMus81
PDS
ATRX WT
ATRX Δ1
F
HeLa LT
ATRXΔ1 siScr
ATRXΔ1 siScr +PDS
ATRXΔ1 siMus81
ATRXΔ1 siMus81 +PDS
DAPI RPA TelC Merge

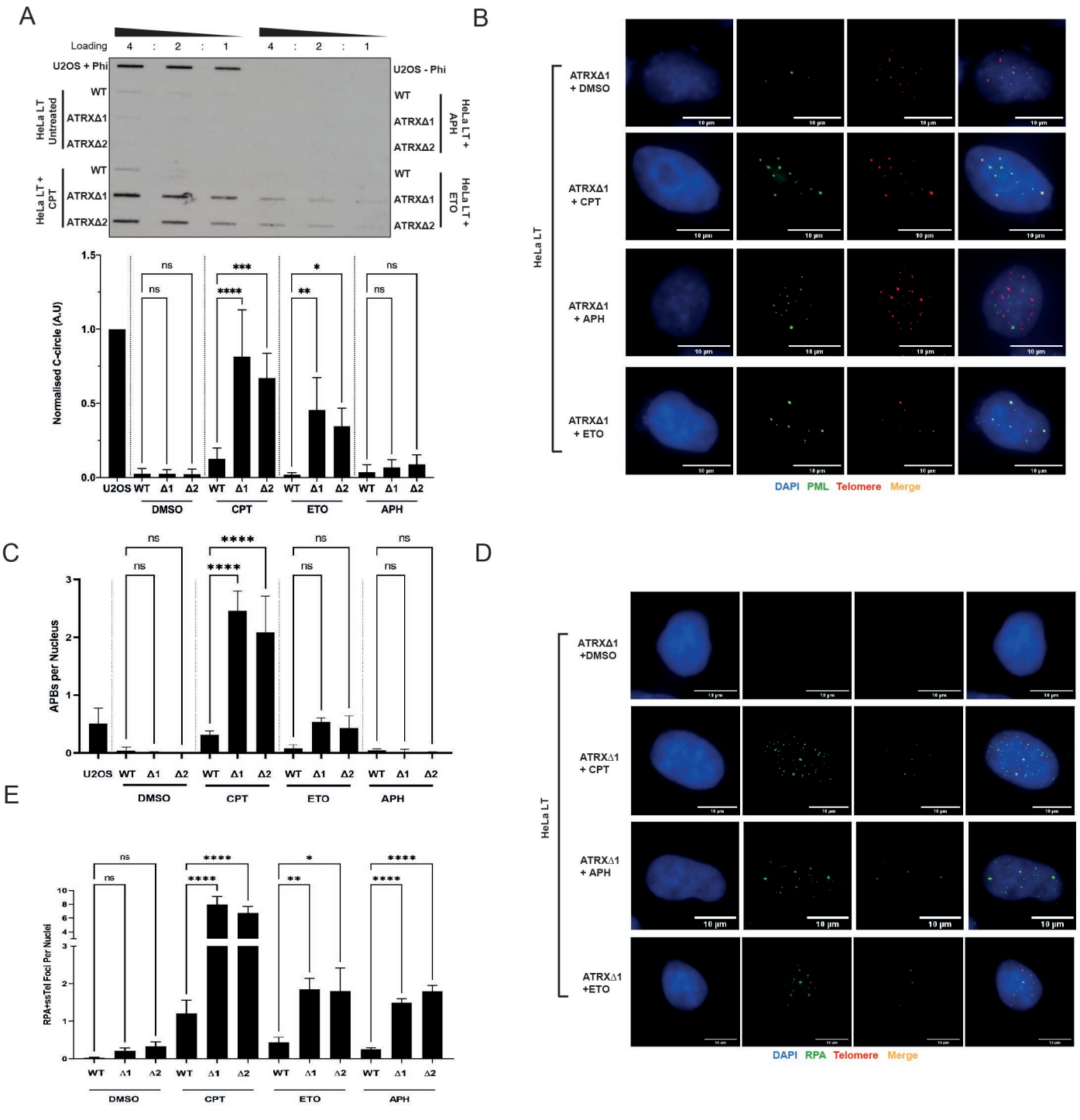
A
Loading
4 : 2 : 1
4 : 2 : 1
U2OS + Phi
U2OS - Phi
HeLa LT Untreated
HeLa LT + CPT
HeLa LT + APH
HeLa LT + ETO
WT
ATRXΔ1
ATRXΔ2
Normalised C-circle (A.U)
U2OS WT Δ1 Δ2 WT Δ1 Δ2 WT Δ1 Δ2 WT Δ1 Δ2
DMSO
CPT
ETO
APH
B
HeLa LT
ATRXΔ1 + DMSO
ATRXΔ1 + CPT
ATRXΔ1 + APH
ATRXΔ1 + ETO
DAPI PML Telomere Merge
C
APBs per Nucleus
D
ATRXΔ1 +DMSO
ATRXΔ1 + CPT
ATRXΔ1 + APH
ATRXΔ1 +ETO
DAPI RPA Telomere Merge
E
RPA+ssTel Foci Per Nuclei

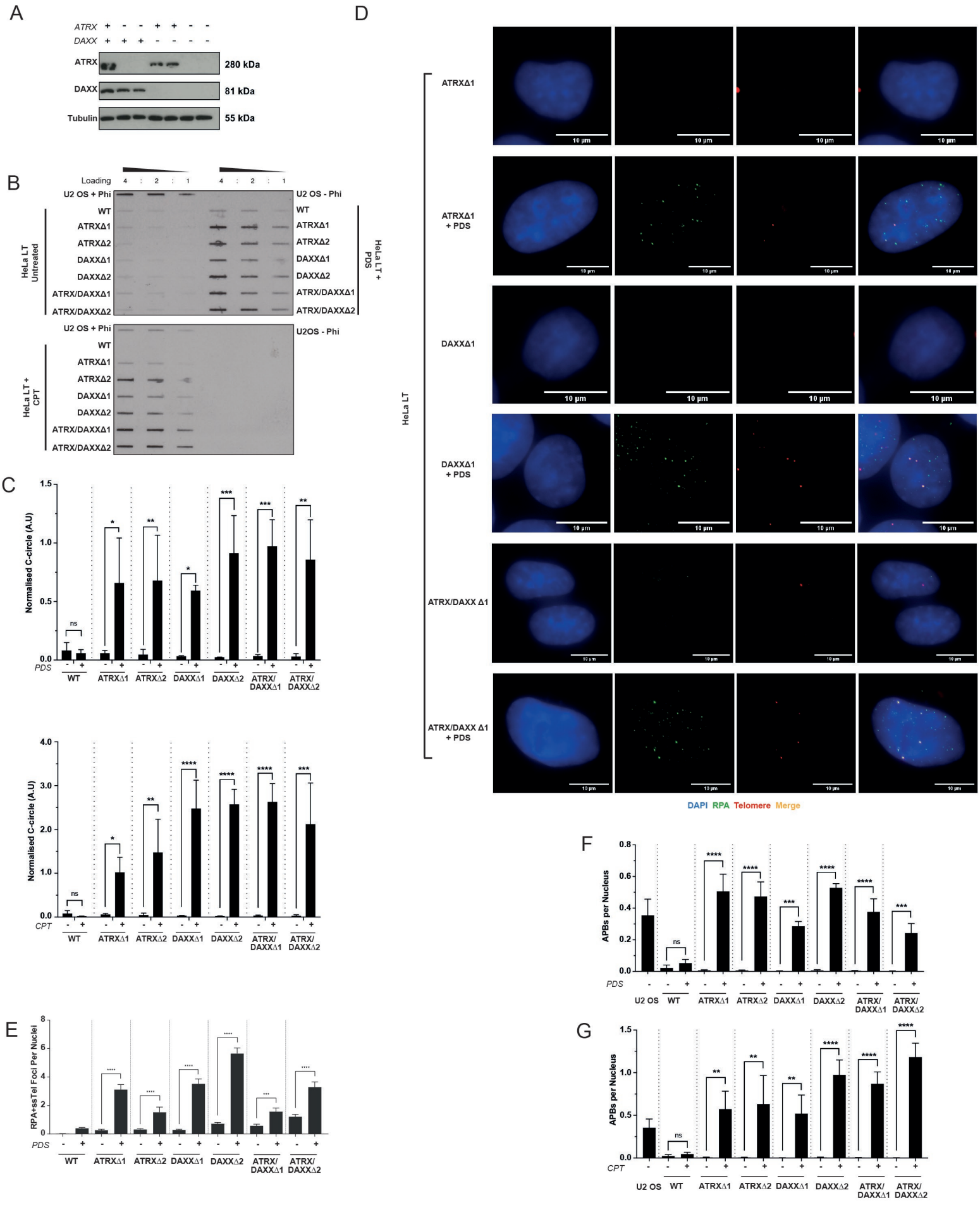
A
ATRX + - - + + - -
DAXX + + + - - - -
ATRX
DAXX
Tubulin
280 kDa
81 kDa
55 kDa
B
Loading 4 : 2 : 1 4 : 2 : 1
U2 OS + Phi
WT
ATRXΔ1
ATRXΔ2
DAXXΔ1
DAXXΔ2
ATRX/DAXXΔ1
ATRX/DAXXΔ2
U2 OS - Phi
U2OS - Phi
HeLa LT Untreated
HeLa LT + PDS
HeLa LT + CPT
C
Normalised C-circle (A.U)
PDS
CPT
WT
ATRXΔ1
ATRXΔ2
DAXXΔ1
DAXXΔ2
ATRX/ DAXXΔ1
ATRX/ DAXXΔ2
D
HeLa LT
ATRXΔ1
ATRXΔ1 + PDS
DAXXΔ1
DAXXΔ1 + PDS
ATRX/DAXX Δ1
ATRX/DAXX Δ1 + PDS
10 µm
DAPI RPA Telomere Merge
E
RPA+ssTel Foci Per Nuclei
F
APBs per Nucleus
U2 OS
G
APBs per Nucleus

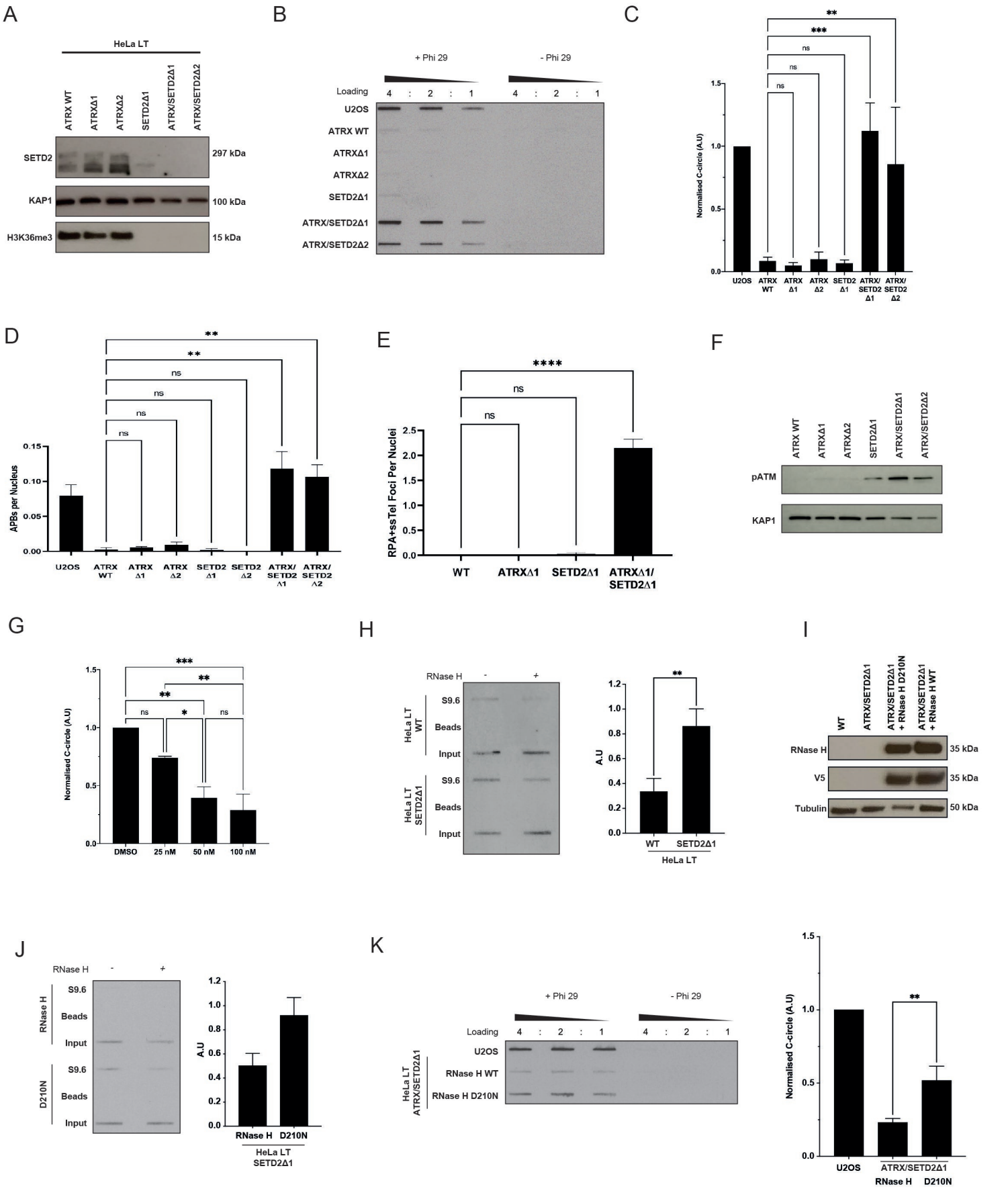
A
HeLa LT
ATRX WT
ATRXΔ1
ATRXΔ2
SETD2Δ1
ATRX/SETD2Δ1
ATRX/SETD2Δ2
SETD2
297 kDa
KAP1
100 kDa
H3K36me3
15 kDa
B
+ Phi 29
- Phi 29
Loading
4 : 2 : 1
U2OS
ATRX WT
ATRXΔ1
ATRXΔ2
SETD2Δ1
ATRX/SETD2Δ1
ATRX/SETD2Δ2
C
Normalised C-circle (A.U)
U2OS
ATRX WT
ATRX Δ1
ATRX Δ2
SETD2 Δ1
ATRX/ SETD2 Δ1
ATRX/ SETD2 Δ2
D
APBs per Nucleus
E
RPA+ssTel Foci Per Nuclei
WT
ATRXΔ1
SETD2Δ1
ATRXΔ1/ SETD2Δ1
F
pATM
KAP1
G
Normalised C-circle (A.U)
DMSO
25 nM
50 nM
100 nM
H
RNase H
HeLa LT WT
HeLa LT SETD2Δ1
S9.6
Beads
Input
A.U
I
WT
ATRX/SETD2Δ1
ATRX/SETD2Δ1 + RNase H D210N
ATRX/SETD2Δ1 + RNase H WT
RNase H
V5
Tubulin
35 kDa
50 kDa
J
D210N
RNase H
D210N
HeLa LT SETD2Δ1
K
HeLa LT ATRX/SETD2Δ1
RNase H WT
RNase H D210N
U2OS
ATRX/SETD2Δ1
RNase H
D210N

A

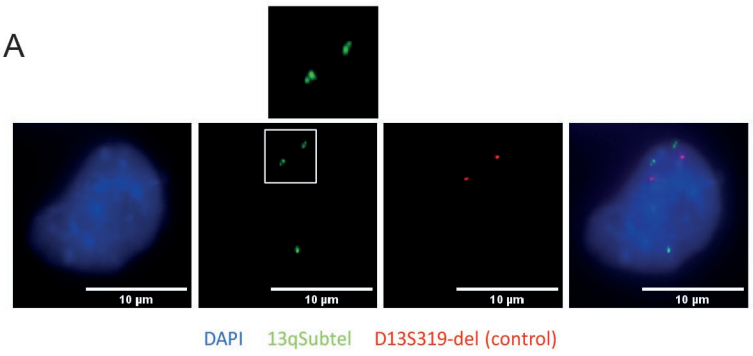
10 µm
10 µm
10 µm
10 µm
DAPI
13qSubtel
D13S319-del (control)

B

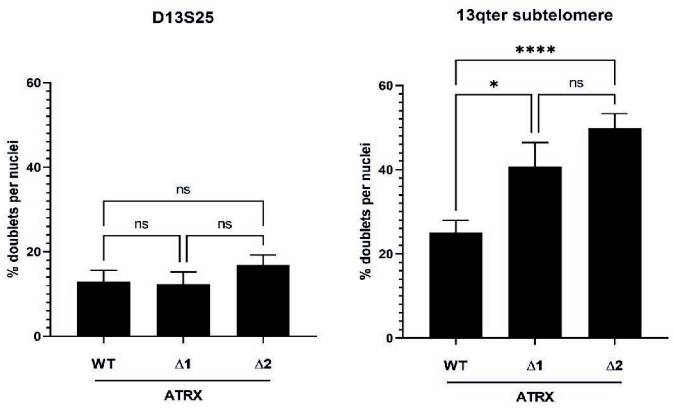
D13S25
% doublets per nuclei
60
40
20
0
ns
ns
ns
WT
Δ1
Δ2
ATRX
13qter subtelomere
****
*
ns
% doublets per nuclei
60
40
20
0
WT
Δ1
Δ2
ATRX

C

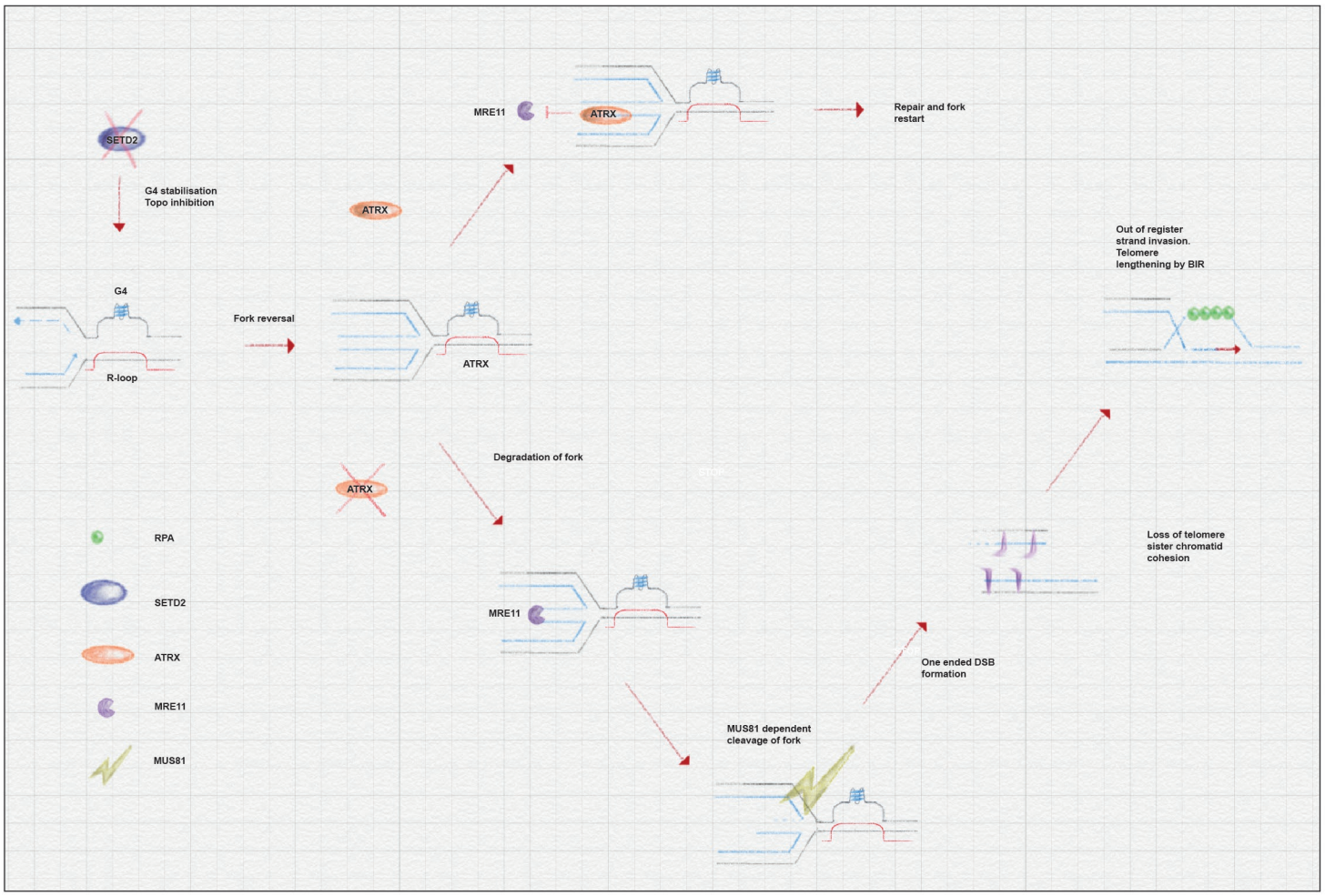
SETD2
G4 stabilisation
Topo inhibition
G4
R-loop
Fork reversal
ATRX
MRE11
ATRX
Repair and fork restart
ATRX
Out of register strand invasion. Telomere lengthening by BIR
Degradation of fork
ATRX
MRE11
Loss of telomere sister chromatid cohesion
One ended DSB formation
MUS81 dependent cleavage of fork
RPA
SETD2
ATRX
MRE11
MUS81

SUPPLEMENTAL INFORMATION

SUPPLEMENTARY TABLE 1 – List of Antibodies Used

ANTIBODY	SOURCE	IDENTIFIER
Alexa Fluor 488 Goat Anti-mouse	Invitrogen	Cat# A11029; 2066710
Alexa Fluor 488 Goat Anti-rabbit	Invitrogen	Cat# A11034; 2256692
Alexa Fluor 568 Goat Anti-mouse	Invitrogen	Cat# A11004; 1906485
Alexa Fluor 568 Goat Anti-rabbit	Invitrogen	Cat# A11011; 1871167
Anti-mouse IgG	Sigma	Cat# A9044; 089M4797V
Anti-rabbit IgG	Sigma	Cat# A6667; SLBX8137
ATRX	Abcam	Cat# ab97508; GR3313858-2
ATRX, clone 39F	Sigma	Cat# MABE1798
DAXX	Sigma	Cat# D7810; 084M4817V
DIG	Roche	Cat# 32871922; 11093274910
H3	Biolegend	Cat# 819414; B303830
H3k36me3	Abcam	Cat# ab9050; GR3307136-2
KAP1	Abcam	Cat# ab10483
MUS81	Santa Cruz	Cat# sc-53382; Clone MTA30 2G-10/3
pATM-S1981	Santa Cruz	Cat# sc-47739; 10H11.E12
PML	Santa Cruz	Cat# dc-966; I1218
PML	Santa Cruz	Cat# sc-5621; D2314
PML	Abcam	Cat# ab53773; GR317758-18
RNase H	Santa Cruz	Cat# sc-101114; D2313
RPA-2	Abcam	Cat# ab2175; GR3224197-4
S9.6	Sigma	Cat# MABE1095

SETD2	GeneTex	Cat# GTX127905
Tubulin	Abcam	Cat# ab7291; GR3197113-3
V5	Cell Signal	Cat# 13202S; D3H8Q

SUPPLEMENTARY TABLE 2 – List of Cell Lines Used

CELL LINE	SOURCE	IDENTIFIER
HeLa LT	*O'Sullivan et al. 2014*	N/A
HeLa LT ATRXΔ1	This Paper	N/A
HeLa LT ATRXΔ2	This Paper	N/A
HeLa LT DAXXΔ1	This Paper	N/A
HeLa LT DAXXΔ2	This Paper	N/A
HeLa LT ATRX/DAXXΔ1	This Paper	N/A
HeLa LT ATRX/DAXXΔ2	This Paper	N/A
HeLa LT SETD2Δ1	This Paper	N/A
HeLa LT ATRX/SETD2Δ1	This Paper	N/A
HeLa LT ATRX/SETD2Δ2	This Paper	N/A
HeLa ST (HeLa H3.3 SNAP)	*Adam et al. 2013*	N/A
G292	ATCC	N/A
SAOS-2	ATCC	N/A
U-2 OS	ATCC	N/A
WI38 VA13 2RA	ATCC	N/A

SUPPLEMENTARY TABLE 3 – List of Oligonucleotides Used

OLIGONUCLEOTIDE	SOURCE	IDENTIFIER
hTeloG: ACACTAAGGTTTGGGTTTGGGTTTGGGTTTGGGTTAG TGT	Life Tech	N/A
hTeloC: TGTTAGGTATCCCTATCCCTATCCCTATCCCTATCCCTA ACA	Life Tech	N/A
GlobinF: CGGCGGCGGGCGGCGCGGGCTGGGCGGCTTCATCCA CGTTCACCTTG	Life Tech	N/A
GlobinR: GCCCGGCCCGCCGCGCCCGTCCCGCCGGAGGAGAAG TCTGCCGTT	Life Tech	N/A
ON-TARGETplus Mus81 siRNA SmartPool	Dharmacon	L-016143-01-0005
TelC DIG Probe: 5'DIG-TTAGGGTTAGGGTTAGGG	IDT	N/A
D13S25, 13q14.3, Red	CytoCell	LPH 043
13qter, 13q34, Green	CytoCell	LPH 043

FIGURE LEGENDS

Supplementary Figure 1. HeLa LT ATRX KO cells show sensitivity to PDS, APH and HU. CellTiterGlo assay following treatment of HeLa LT ATRX Wild Type and KO cells with A) PDS, B) APH and C) HU at the doses shown. IC50 values are indicated, n=3.

Supplementary Figure 2. PDS Treatment Induces ATRX Foci Formation. A) ImmunoFISH assay quantification showing treatment of HeLa LT WT cells with PDS induces an increase in ATRX foci formation at telomeres, >100 nuclei analysed across 2 biological replicates. ****p < 0.00001, determined by unpaired Student's t test. B) Representative ImmunoFISH images.

Supplementary Figure 3. Treatment with PDS in ATRX KO cells leads to telomere clustering. A) Intensity of telomere foci. Foci considered intense are shown above dotted line 15000 (a.u.). Significance donates increase in intense foci. Data is collation of 3 biological replicates each with over 100 nuclei analysed. ****p < 0.00001, determined by one-way ANOVA. B) Quantitation of telomere number per nucleus. Data is collation of 3 biological replicates each with over 150 nuclei analysed. ****p < 0.00001.

Supplementary Figure 4. RPA coincident with single stranded telomeric sequence is a marker of ALT activity. A) Representative image showing RPA coincident with telomeric sequence in ALT positive U-2 OS and WI38 VA13 2RA cells, >100 nuclei analysed across 3 biological replicates. B) Quantification of RPA+ssTel in a panel of ALT, non-ALT, and ATRX re-expressed cell lines. ****p < 0.00001, determined by one-way ANOVA. C) WI38 VA13 2RA cells treated with RNaseA and RNaseH did not show reduction in telomere foci, >50 nuclei analysed across 2 biological replicates. ns signifies p > 0.05, determined by one-way ANOVA.

Supplementary Figure 5. Telomere length and heterogeneity increases following treatment with PDS amd CPT. A) Ratio of telomere repeats to the single copy gene beta-globin (T/S ratio) following the addition of PDS as assessed by mm-qPCR in HeLa LT ATRX wildtype or ATRX KO clones, n=6. *p < 0.05, ***p < 0.0001, determined by unpaired Student's t test. B) Terminal restriction fragment (TRF) assay following treatment with CPT. Telomere length

heterogeneity was calculated using TeloMetric software, n=2. **p < 0.001, determined by one-way ANOVA.

Supplementary Figure 6. Treatment with PDS in combination with ATRX loss triggers ALT markers in HeLa standard telomere length (ST) cells. A) Immunoblot of shScr and shATRX populations in HeLa ST cells. B-C) C-circle blot and quantification showing HeLa ST shScr and shATRX with CPT treatment at indicated doses in nM, n=2. D-E) RPA ssTel representative images and quantification showing HeLa H3.3 SNAP shScr and shATRX with PDS treatment, >100 nuclei analysed across 3 biological replicates. *p < 0.05, ****p < 0.00001, determined by one-way ANOVA.

Supplementary Figure 7. Effect of Triptolide Treatment on Cell Cycle. A) Representative C-circle assay in HeLa LT ATRX/SETD2 knockout cells after 24 hours treatment with 25, 50 and 100 nM Triptolide. B-E) Representative plots of PI staining for the doses of triptolide indicated. F) Quantification of cell cycle phases by PI staining and FACs analysis upon treatment of indicated doses of triptolide in the HeLa LT ATRX/SETD2 knockout cells, n=2.

A

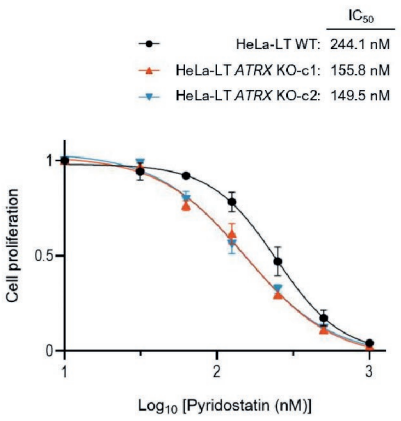
IC50
HeLa-LT WT: 244.1 nM
HeLa-LT ATRX KO-c1: 155.8 nM
HeLa-LT ATRX KO-c2: 149.5 nM
Cell proliferation
Log10 [Pyridostatin (nM)]

B

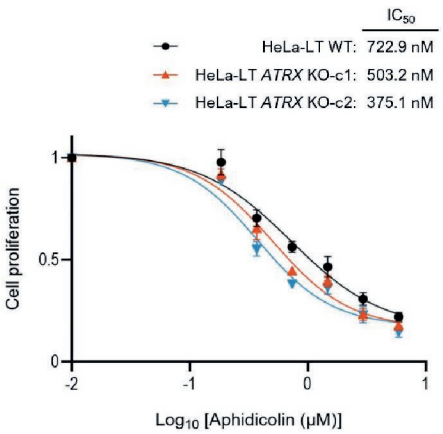
IC50
HeLa-LT WT: 722.9 nM
HeLa-LT ATRX KO-c1: 503.2 nM
HeLa-LT ATRX KO-c2: 375.1 nM
Cell proliferation
Log10 [Aphidicolin (μM)]

C

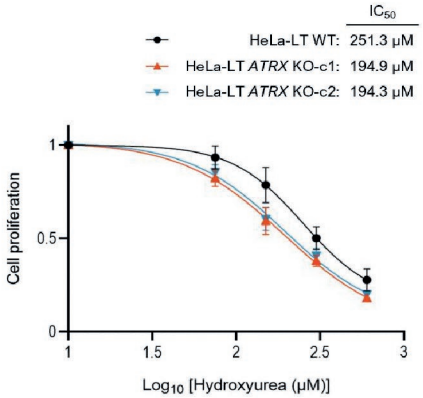
IC50
HeLa-LT WT: 251.3 μM
HeLa-LT ATRX KO-c1: 194.9 μM
HeLa-LT ATRX KO-c2: 194.3 μM
Cell proliferation
Log10 [Hydroxyurea (μM)]

A

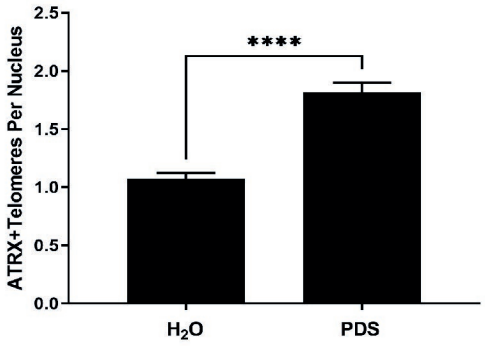
ATRX+Telomeres Per Nucleus
2.5
2.0
1.5
1.0
0.5
0.0
****
H2O
PDS

B

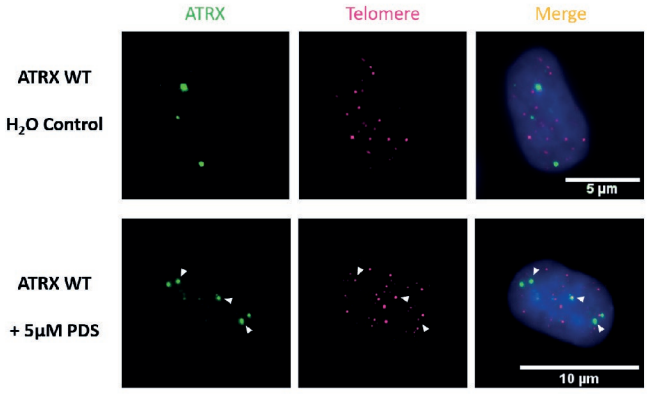
ATRX
Telomere
Merge
ATRX WT
H2O Control
5 µm
ATRX WT
+ 5µM PDS
10 µm

A

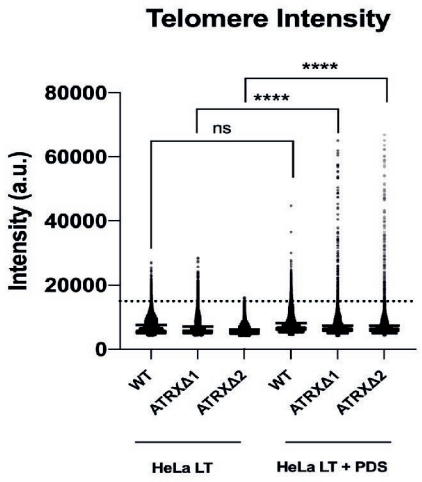
Telomere Intensity
Intensity (a.u.)
80000
60000
40000
20000
0
****
****
ns
WT
ATRXΔ1
ATRXΔ2
WT
ATRXΔ1
ATRXΔ2
HeLa LT
HeLa LT + PDS

B

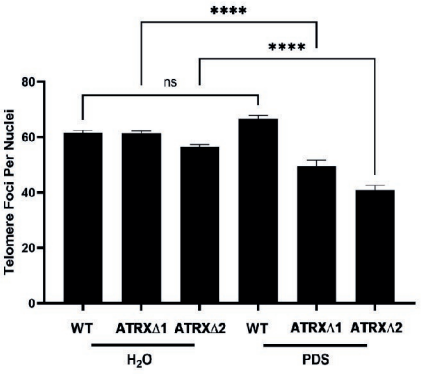
****
****
ns
Telomere Foci Per Nuclei
80
60
40
20
0
WT
ATRXΔ1
ATRXΔ2
WT
ATRXΔ1
ATRXΔ2
H2O
PDS

A

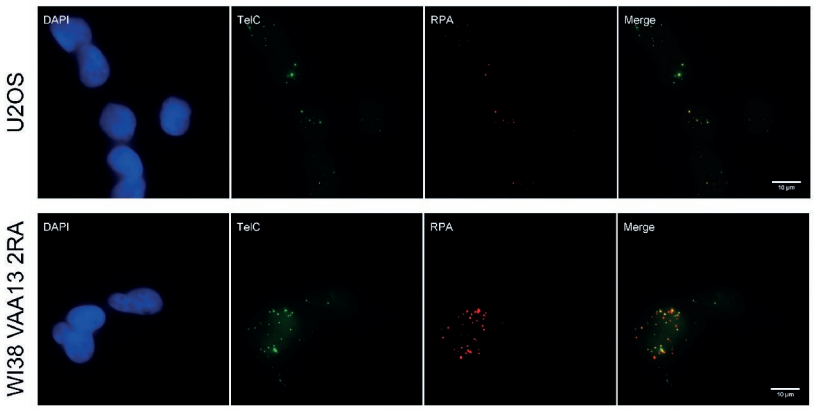
U2OS
WI38 VAA13 2RA
DAPI
TelC
RPA
Merge

B

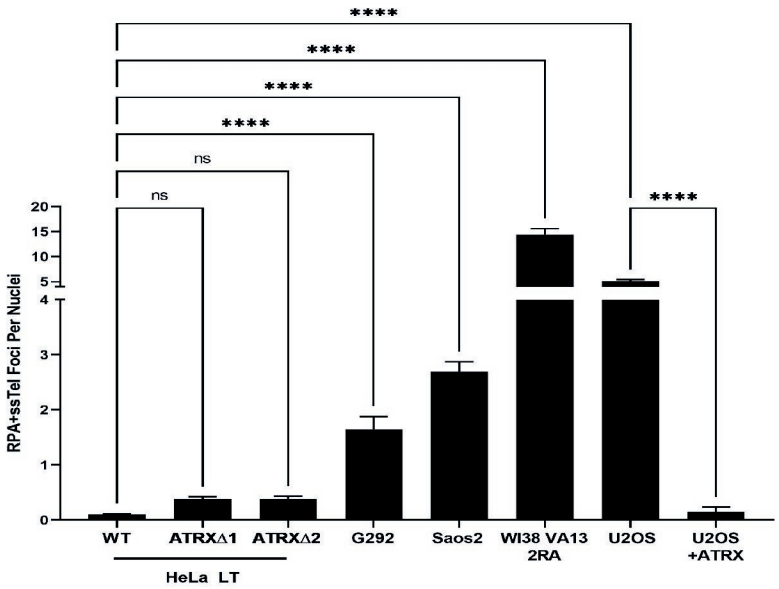
RPA+ssTel Foci Per Nuclei
****
****
****
****
ns
ns
****
WT
ATRXΔ1
ATRXΔ2
G292
Saos2
WI38 VA13 2RA
U2OS
U2OS +ATRX
HeLa LT

C

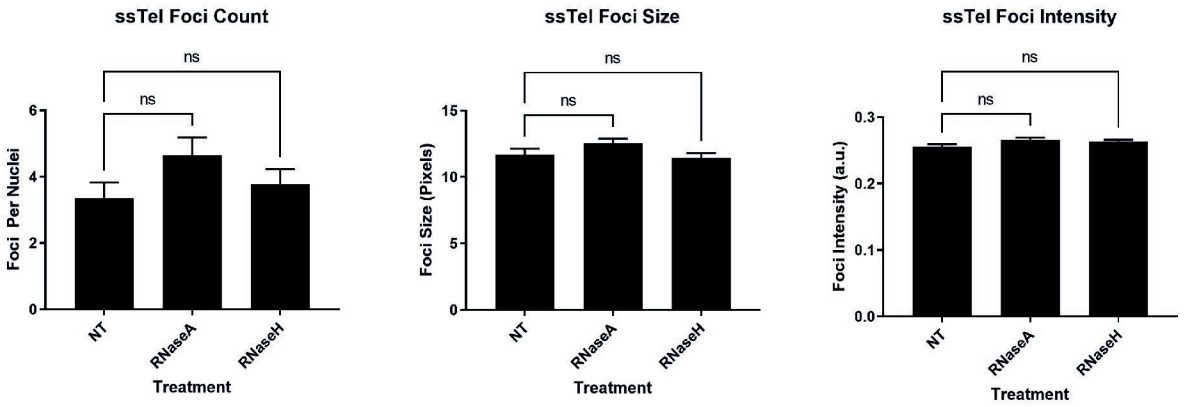
ssTel Foci Count
Foci Per Nuclei
ssTel Foci Size
Foci Size (Pixels)
ssTel Foci Intensity
Foci Intensity (a.u.)
ns
NT
RNaseA
RNaseH
Treatment

FIGURE S5

A

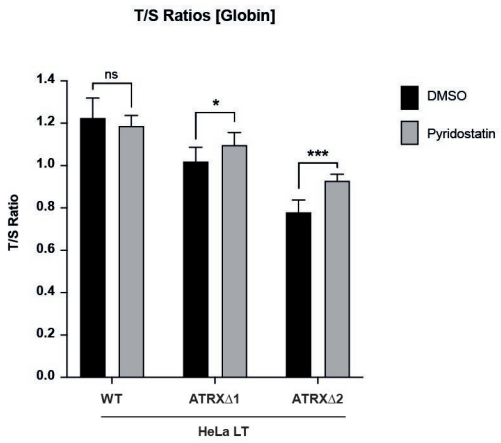
T/S Ratios [Globin]
T/S Ratio
1.4
1.2
1.0
0.8
0.6
0.4
0.2
0.0
ns
*
***
DMSO
Pyridostatin
WT
ATRXΔ1
ATRXΔ2
HeLa LT

B

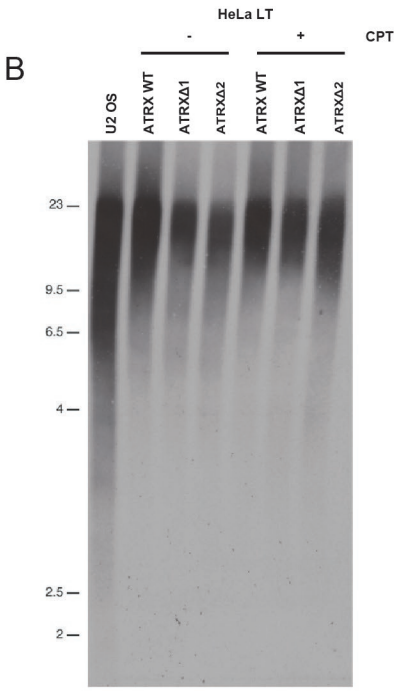
HeLa LT
-
+
CPT
U2 OS
ATRX WT
ATRXΔ1
ATRXΔ2
ATRX WT
ATRXΔ1
ATRXΔ2
23
9.5
6.5
4
2.5
2

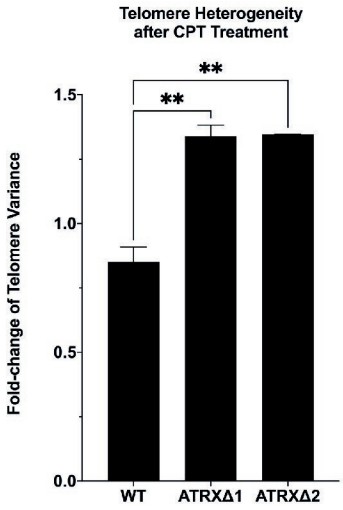
Telomere Heterogeneity
after CPT Treatment
Fold-change of Telomere Variance
1.5
1.0
0.5
0.0
**
**
WT
ATRXΔ1
ATRXΔ2

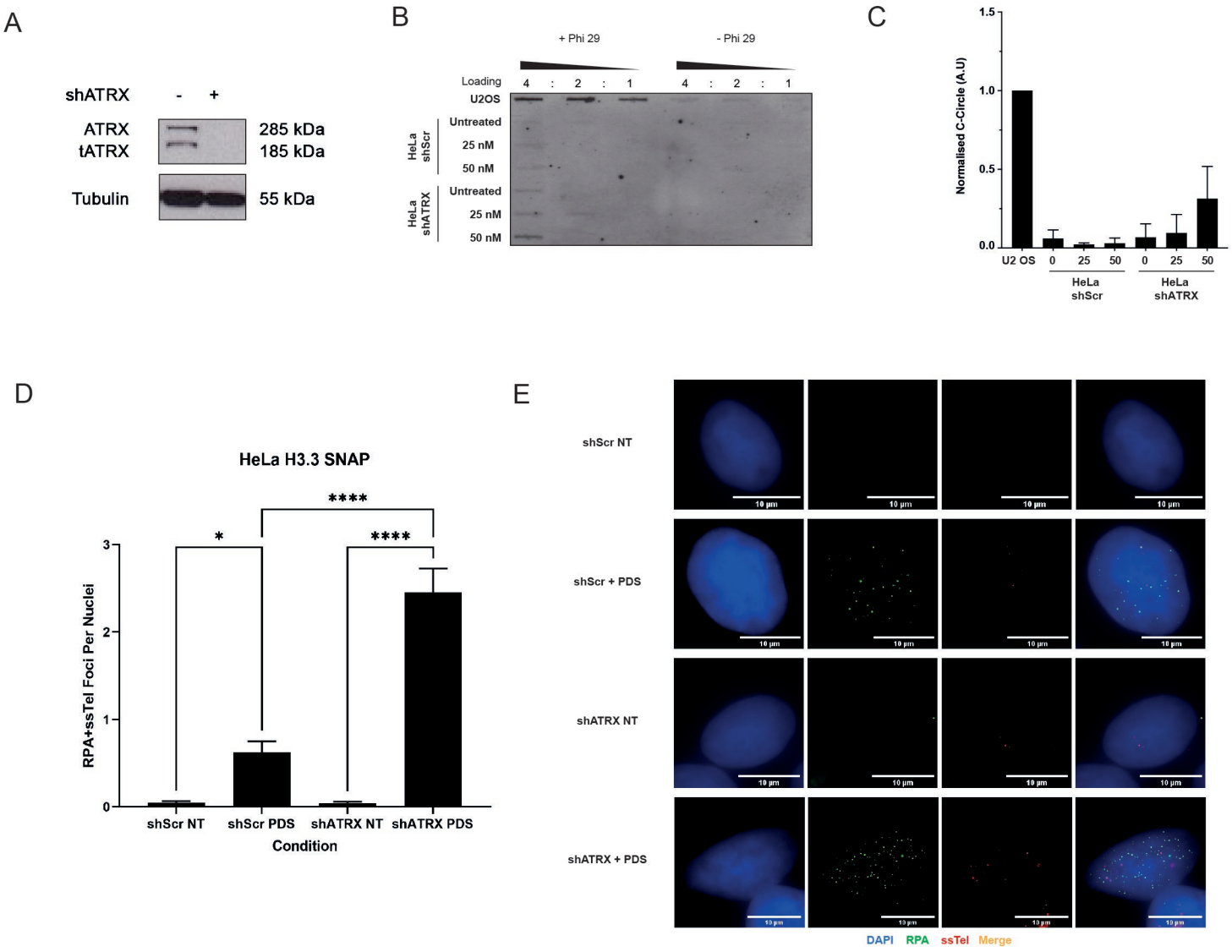
A
shATRX - +
ATRX 285 kDa
tATRX 185 kDa
Tubulin 55 kDa
B
+ Phi 29
- Phi 29
Loading 4 : 2 : 1 4 : 2 : 1
U2OS
HeLa shScr
Untreated
25 nM
50 nM
HeLa shATRX
Untreated
25 nM
50 nM
C
Normalised C-Circle (A.U)
1.5
1.0
0.5
0.0
U2 OS 0 25 50 0 25 50
HeLa shScr
HeLa shATRX
D
HeLa H3.3 SNAP
RPA+ssTel Foci Per Nuclei
3
2
1
0
*
****
****
shScr NT
shScr PDS
shATRX NT
shATRX PDS
Condition
E
shScr NT
shScr + PDS
shATRX NT
shATRX + PDS
10 µm
DAPI RPA ssTel Merge

A

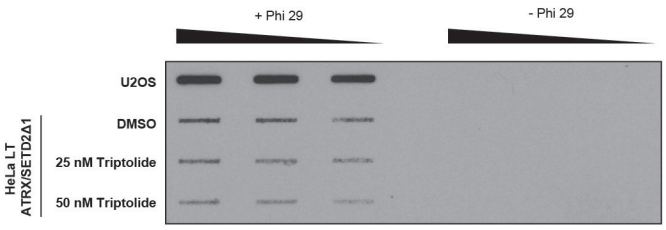
+ Phi 29
- Phi 29
U2OS
DMSO
25 nM Triptolide
50 nM Triptolide
HeLa LT ATRX/SETD2Δ1

B

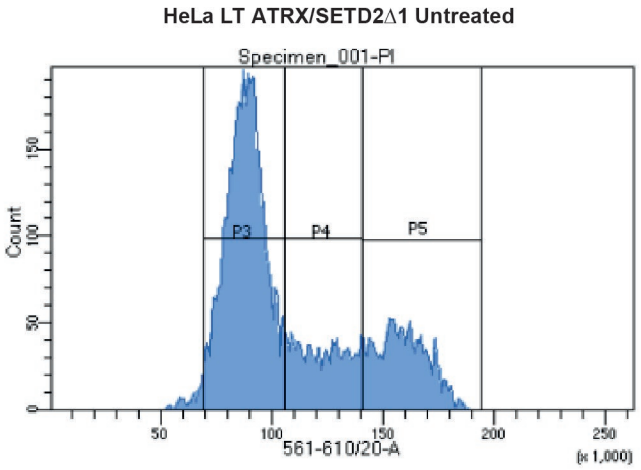
HeLa LT ATRX/SETD2Δ1 Untreated
Specimen_001-P1
Count
P3
P4
P5
561-610/20-A
(x 1,000)

C

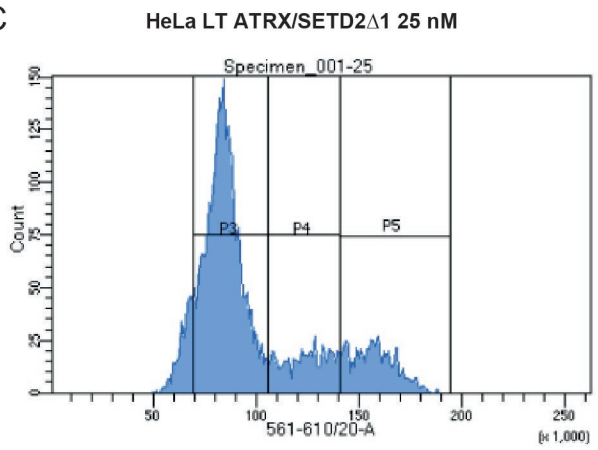
HeLa LT ATRX/SETD2Δ1 25 nM
Specimen_001-25
Count
P3
P4
P5
561-610/20-A
(x 1,000)

D

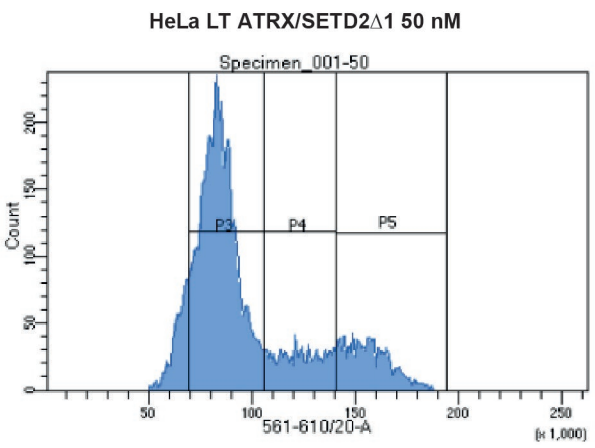
HeLa LT ATRX/SETD2Δ1 50 nM
Specimen_001-50
Count
P3
P4
P5
561-610/20-A
(x 1,000)

E

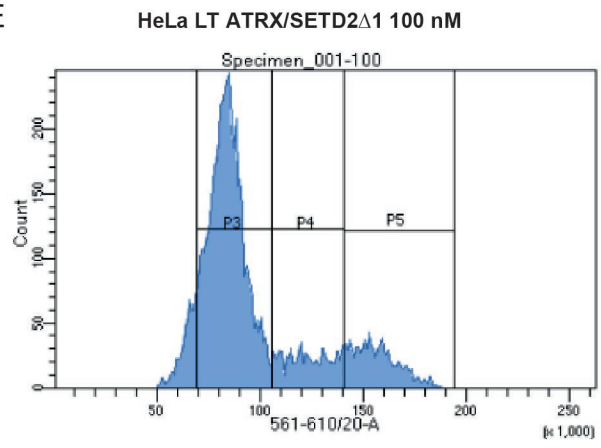
HeLa LT ATRX/SETD2Δ1 100 nM
Specimen_001-100
Count
P3
P4
P5
561-610/20-A
(x 1,000)

F

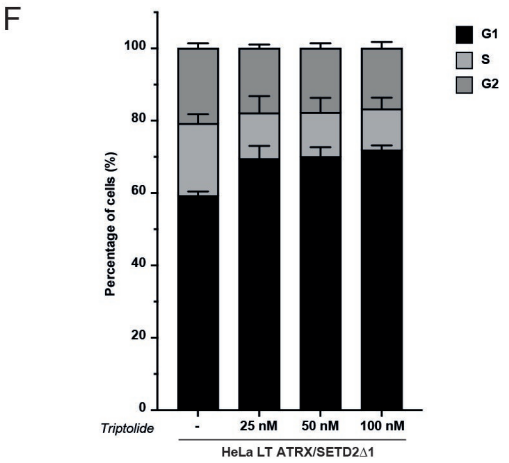
G1
S
G2
Percentage of cells (%)
Triptolide
-
25 nM
50 nM
100 nM
HeLa LT ATRX/SETD2Δ1

Figures

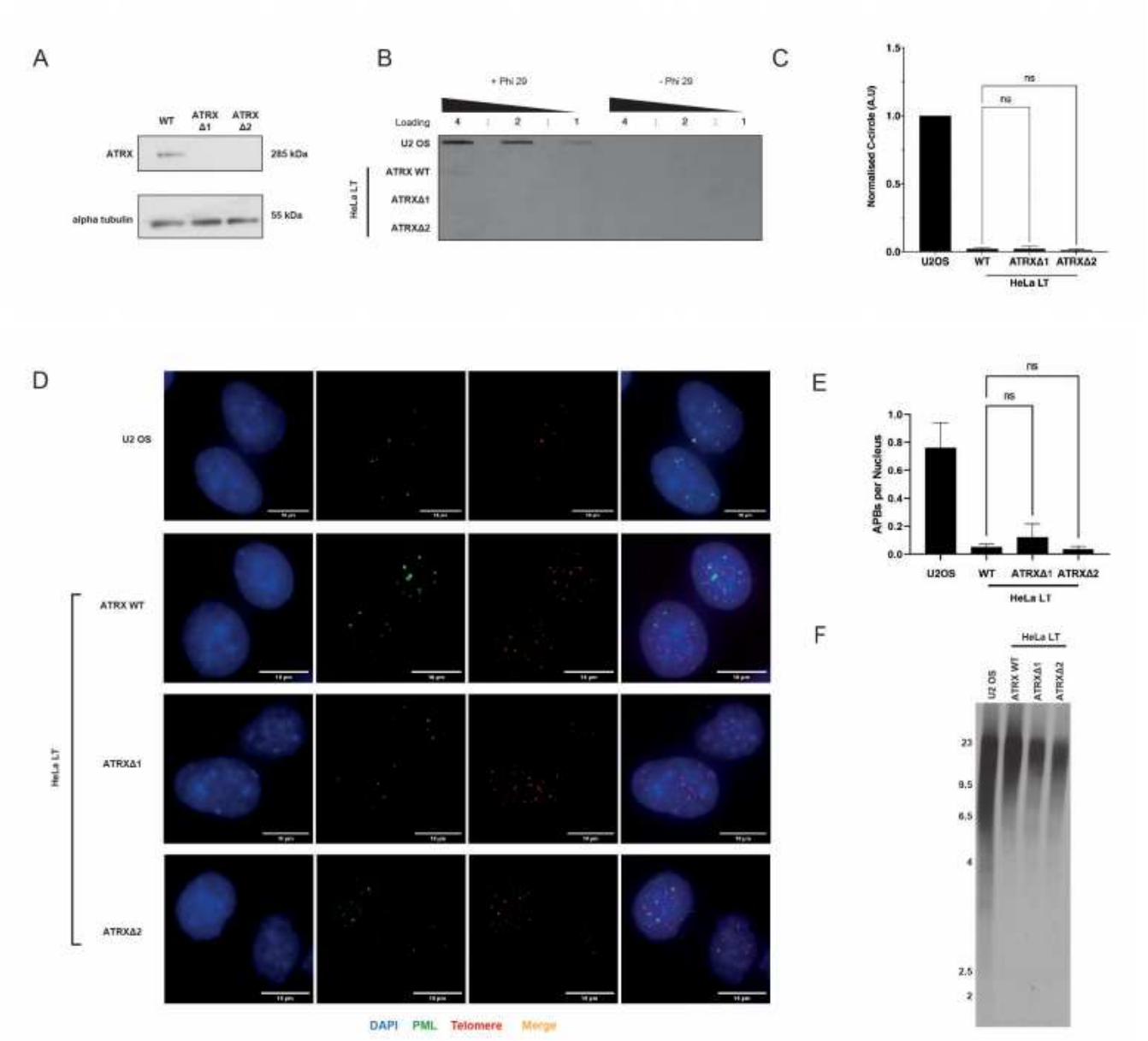

Figure 1

Loss of ATRX alone is insufficient to trigger the ALT pathway.

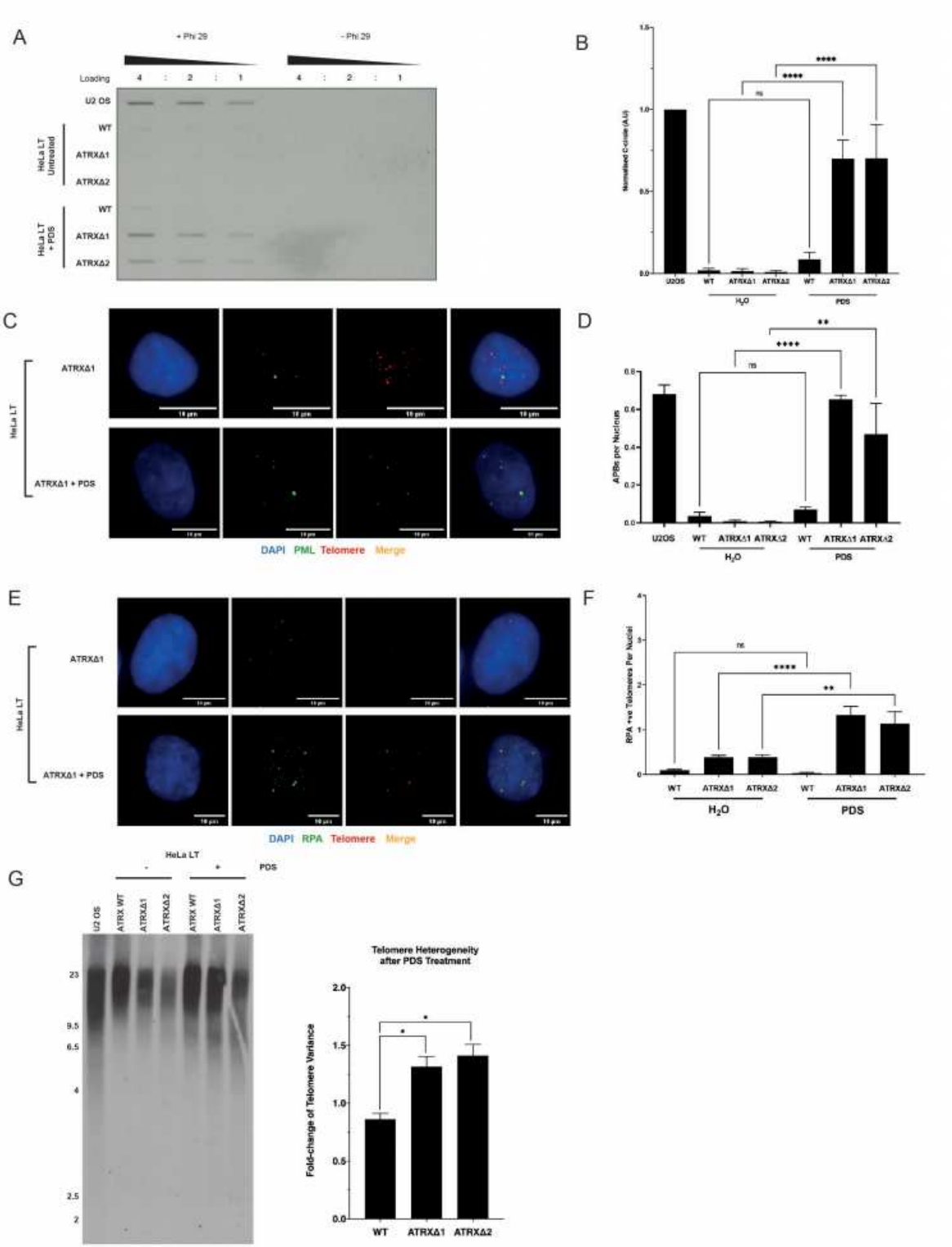

Figure 2

Treatment with PDS in combination with ATRX loss triggers ALT markers.

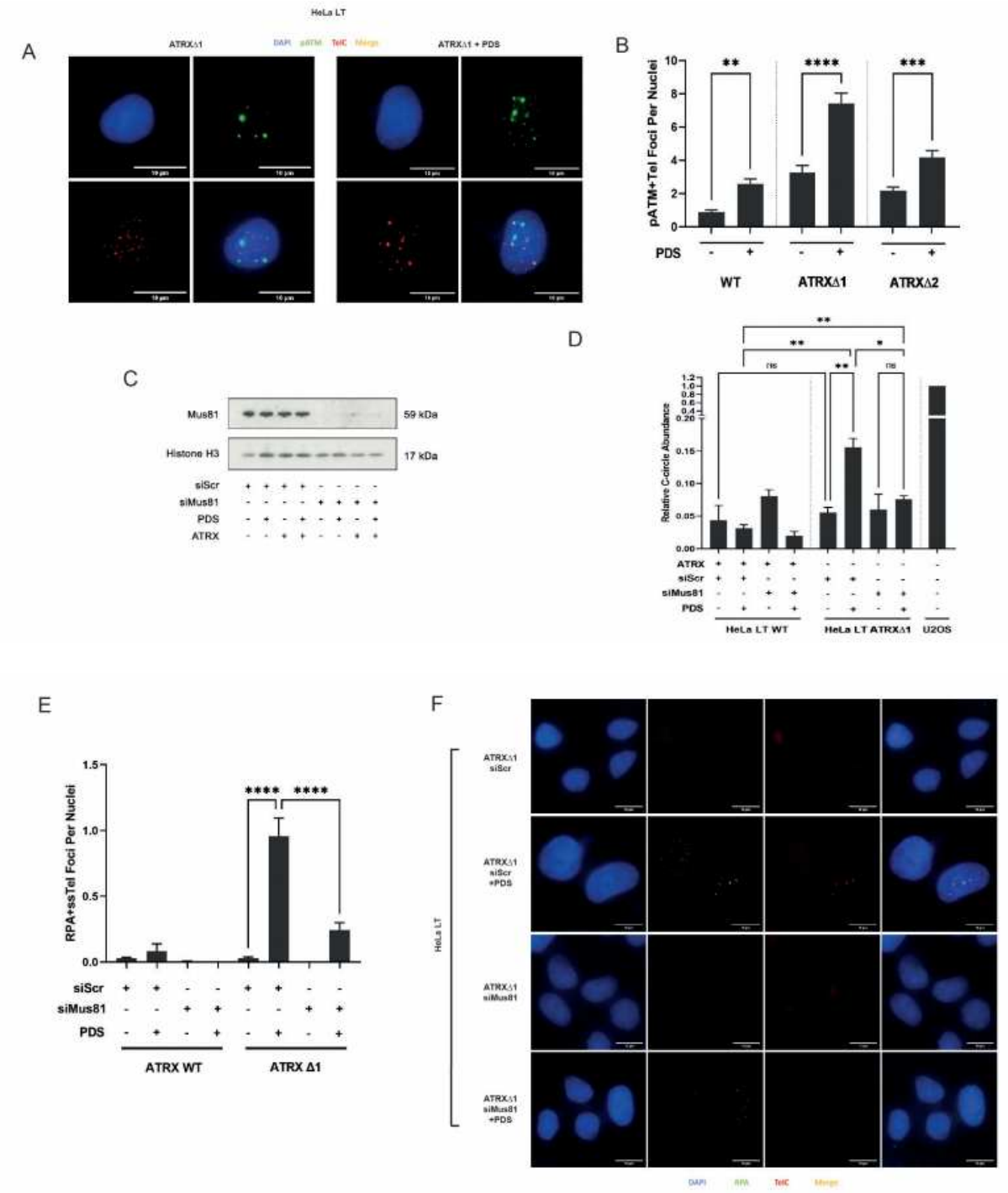

Figure 3

PDS induced ALT markers require replication fork collapse.

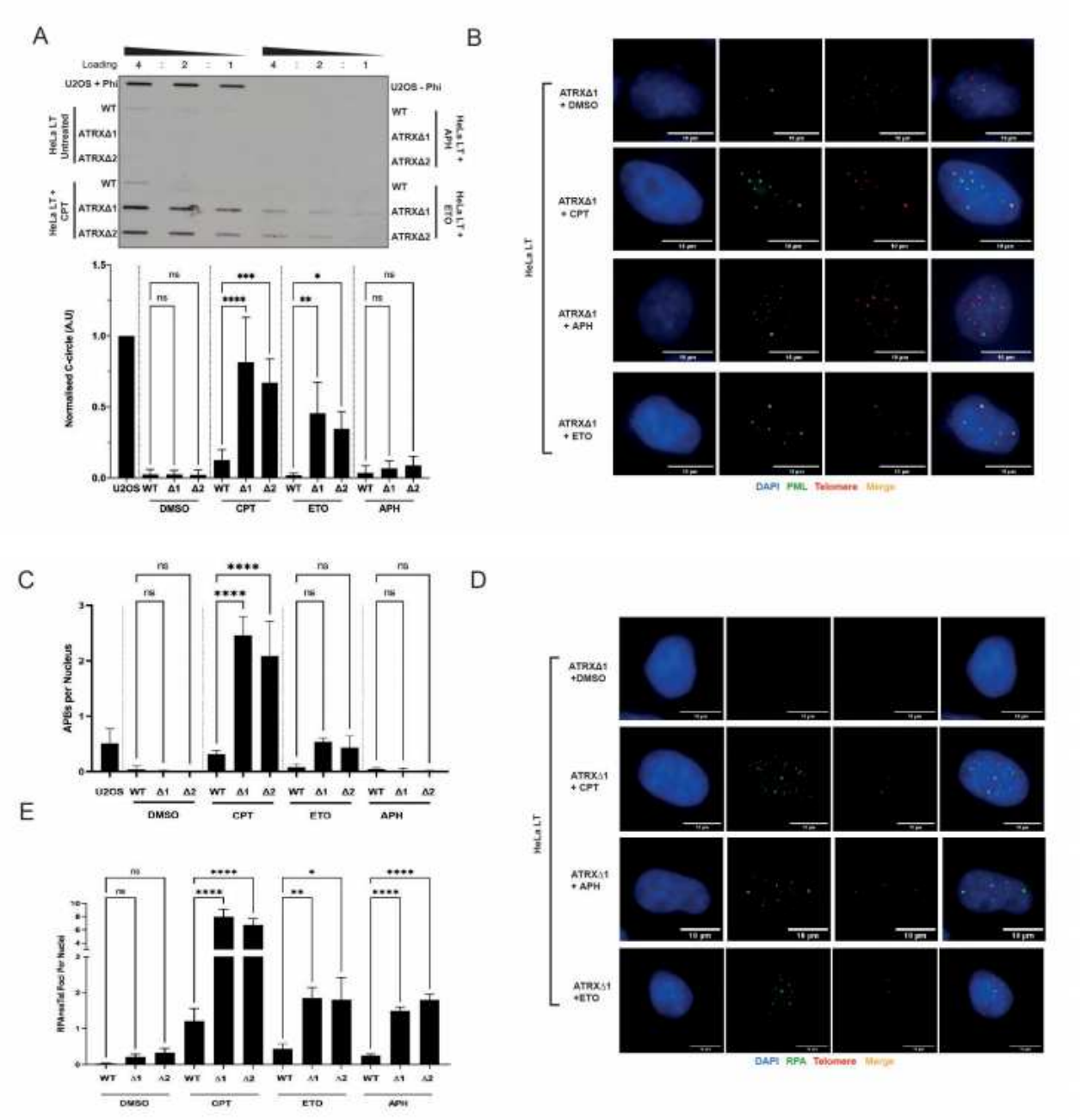

Figure 4

A variety of genotoxic agents induce markers of ALT in ATRX deficient cells.

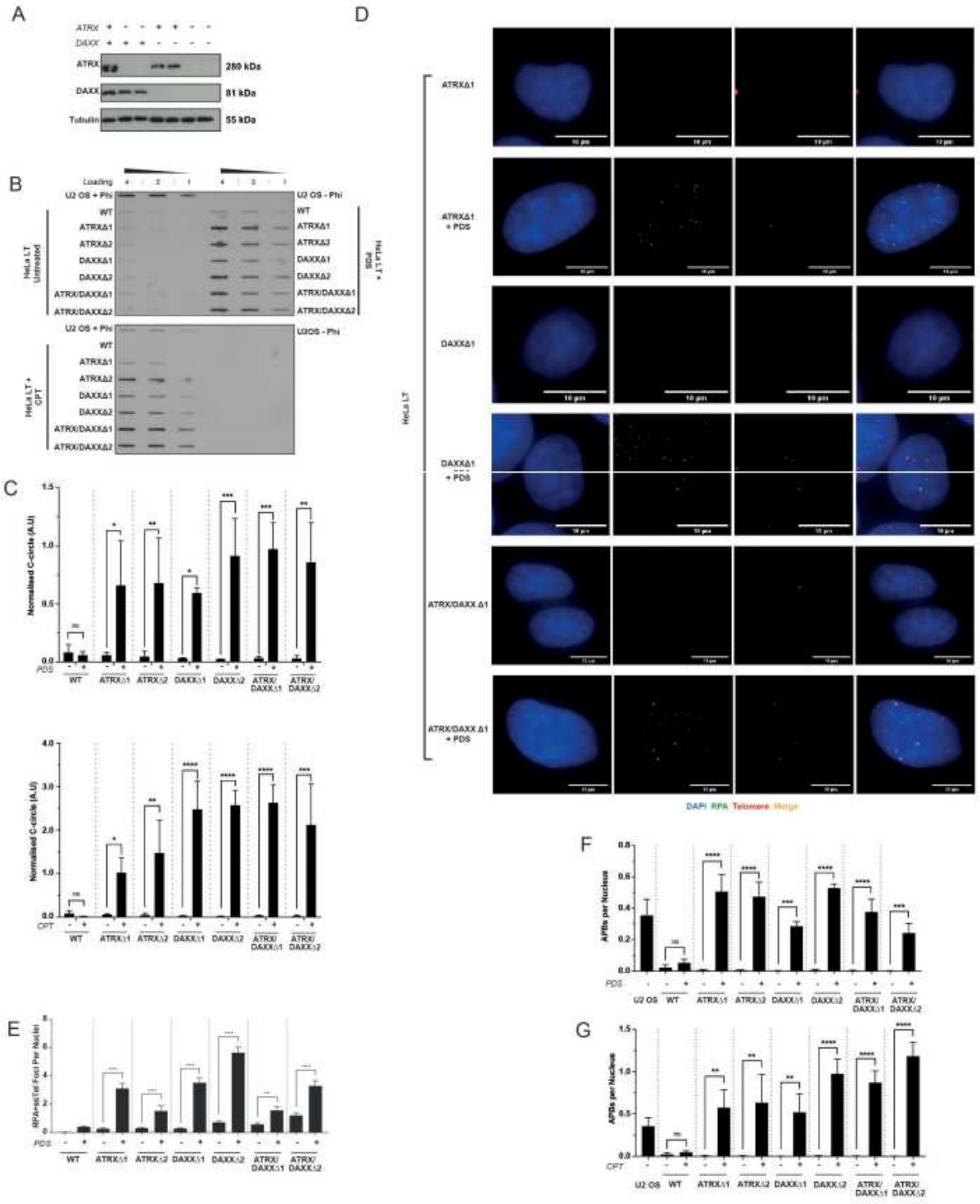

Figure 5

ATRX and DAXX act epistatically in the suppression of induced ALT.

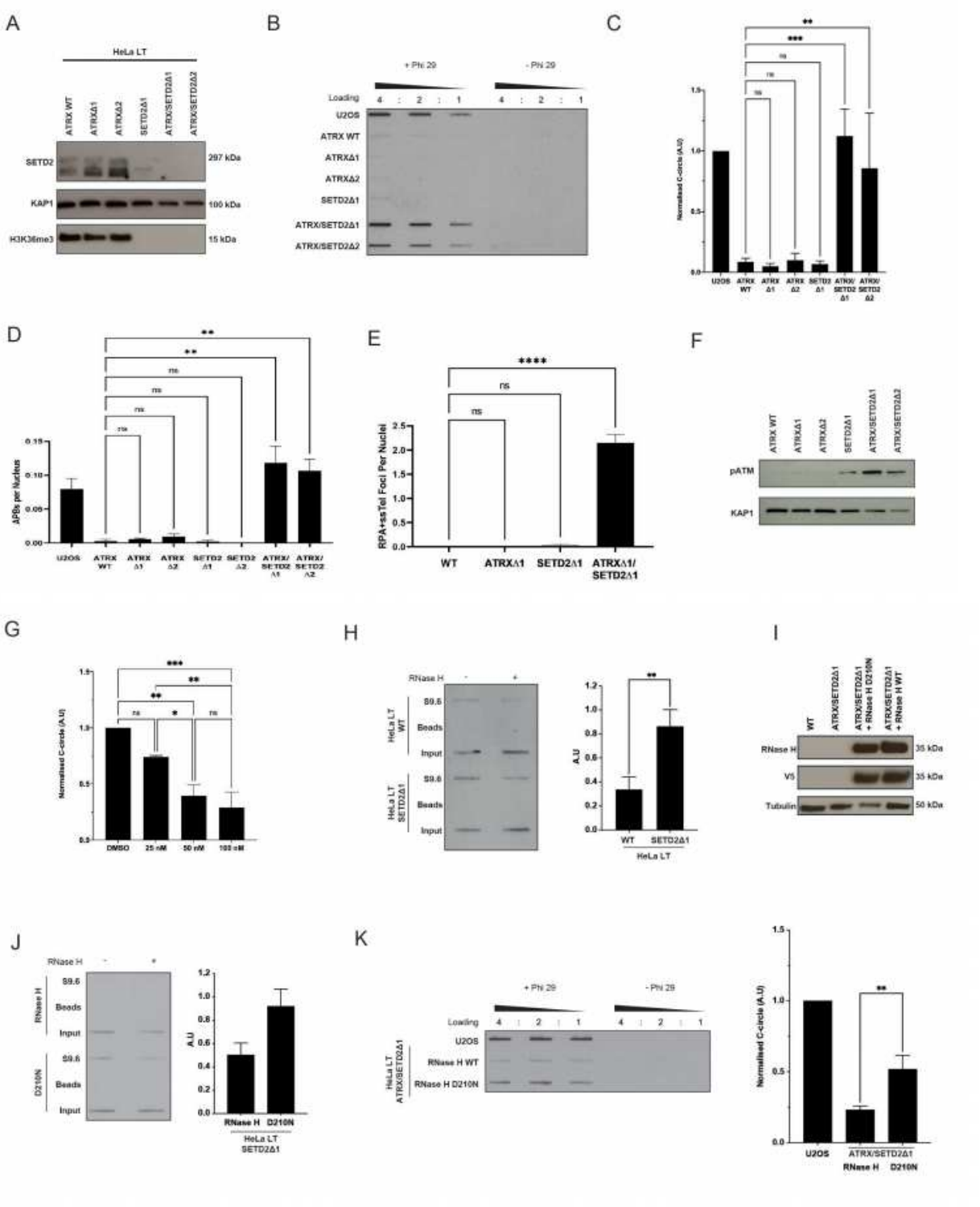

Figure 6

SETD2 loss in combination with ATRX loss triggers markers of the ALT pathway.

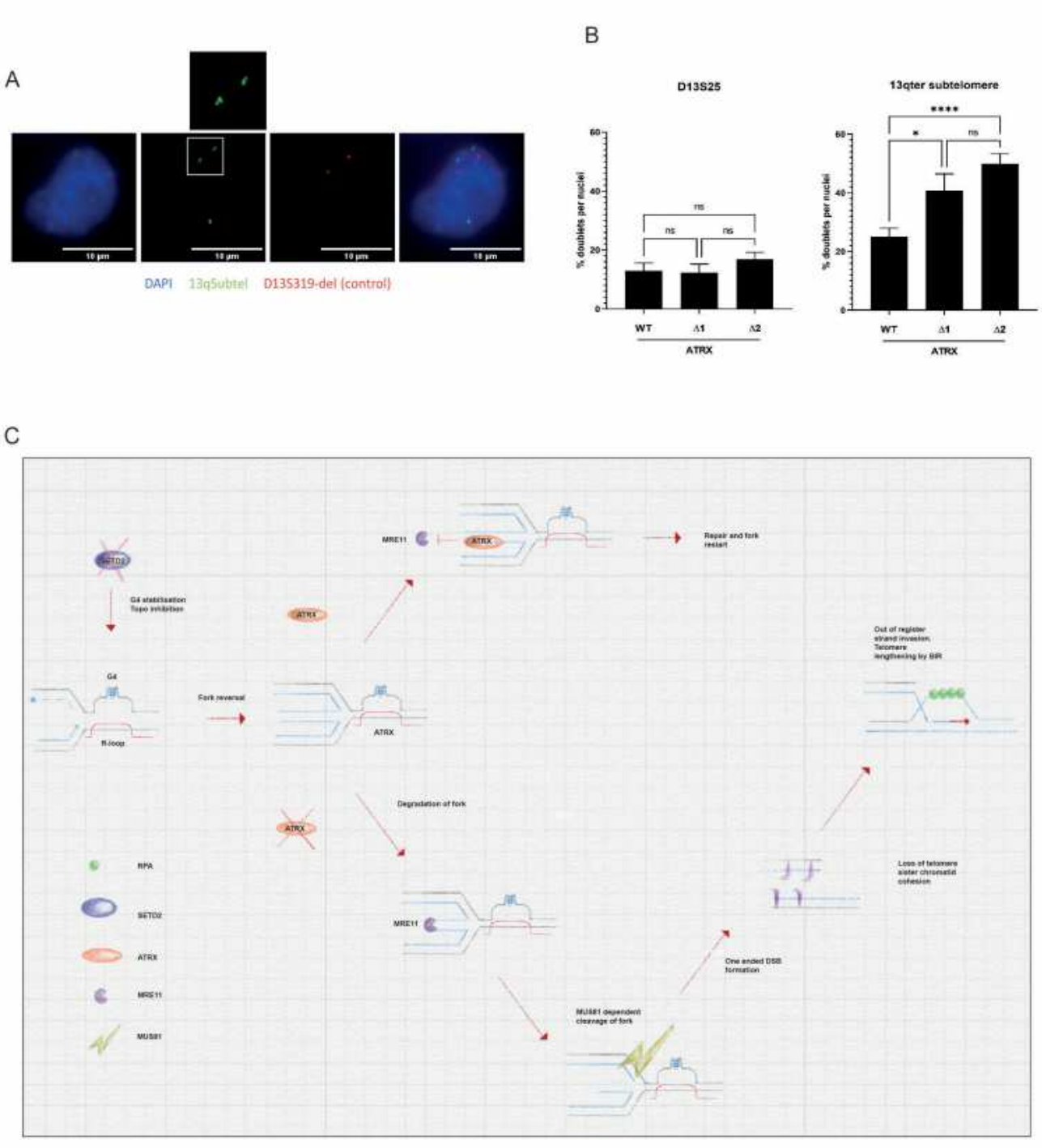

Figure 7

Loss of ATRX induces loss of telomere sister chromatid cohesion.